

# Exactly separable version of the Bohr Hamiltonian with the Davidson potential

Dennis Bonatsos<sup>a1</sup>, E. A. McCutchan<sup>b2</sup>, N. Minkov<sup>c3</sup>, R.F. Casten<sup>b4</sup>, P. Yotov<sup>c5</sup>, D. Lenis<sup>a6</sup>, D. Petrellis<sup>a7</sup>, I. Yigitoglu<sup>d8</sup>

<sup>a</sup> Institute of Nuclear Physics, N.C.S.R. “Demokritos”,  
GR-15310 Aghia Paraskevi, Attiki, Greece

<sup>b</sup> Wright Nuclear Structure Laboratory, Yale University,  
New Haven, Connecticut 06520-8124, USA

<sup>c</sup> Institute of Nuclear Research and Nuclear Energy,  
72 Tzarigrad Road, 1784 Sofia, Bulgaria

<sup>d</sup> Hasan Ali Yucel Faculty of Education, Istanbul University,  
TR-34470 Beyazit, Istanbul, Turkey

## Abstract

An exactly separable version of the Bohr Hamiltonian is developed using a potential of the form  $u(\beta) + u(\gamma)/\beta^2$ , with the Davidson potential  $u(\beta) = \beta^2 + \beta_0^4/\beta^2$  (where  $\beta_0$  is the position of the minimum) and a stiff harmonic oscillator for  $u(\gamma)$  centered at  $\gamma = 0^\circ$ . In the resulting solution, called exactly separable Davidson (ES-D), the ground state band,  $\gamma$  band and  $0_2^+$  band are all treated on an equal footing. The bandheads, energy spacings within bands, and a number of interband and intraband  $B(E2)$  transition rates are well reproduced for almost all well-deformed rare earth and actinide nuclei using two parameters ( $\beta_0$ ,  $\gamma$  stiffness). Insights regarding the recently found correlation between  $\gamma$  stiffness and the  $\gamma$ -bandhead energy, as well as the long standing problem of producing a level scheme with Interacting Boson Approximation SU(3) degeneracies from the Bohr Hamiltonian, are also obtained.

PACS: 21.60.Ev, 21.60.Fw, 21.10.Re

Section: Nuclear structure

---

<sup>1</sup>e-mail: bonat@inp.demokritos.gr

<sup>2</sup>e-mail: elizabeth.ricard-mccutchan@yale.edu

<sup>3</sup>e-mail: nminkov@inrne.bas.bg

<sup>4</sup>e-mail: richard.casten@yale.edu

<sup>5</sup>e-mail: pyotov@inrne.bas.bg

<sup>6</sup>e-mail: lenis@inp.demokritos.gr

<sup>7</sup>e-mail: petrellis@inp.demokritos.gr

<sup>8</sup>e-mail: yigitoglu@istanbul.edu.tr

# 1 Introduction

The Bohr Hamiltonian [1] has been at the foundation of the collective model description of nuclei for over fifty years. Numerous solutions have been proposed since its derivation by choosing different forms of the potential  $V(\beta, \gamma)$  and solving the corresponding eigenvalue equation either analytically or approximately. Recently, this approach has undergone renewed interest, due in part, to the development of the concept of critical point symmetries (CPS). These models, E(5) [2] and X(5) [3], are special solutions of the Bohr Hamiltonian designed to describe nuclei at the critical point of the shape/phase transition between vibrational and  $\gamma$ -soft or axially symmetric deformed structures, respectively.

In E(5) [2], a  $\gamma$ -independent potential of the form  $u(\beta)$  is used, leading to exact separation of  $\beta$  from  $\gamma$  and the Euler angles [4], while in X(5) [3] a potential of the form  $u(\beta) + u(\gamma)$  is assumed, leading to an approximate separation of variables in the special case of  $\gamma \approx 0^\circ$ , achieved by  $u(\gamma)$  being a stiff harmonic oscillator centered at  $\gamma = 0^\circ$ . In both E(5) and X(5) an infinite square well potential is used as  $u(\beta)$ , in accordance with growing evidence from microscopic calculations [5, 6, 7] that the potential at the transition point between different shapes should be flat. Model predictions for energy spectra and  $B(E2)$  transition rates are parameter free (up to overall scale factors) in E(5) [2], while in X(5) the predictions related to the ground state band and the excited  $0^+$  bands are parameter free, but  $\gamma$  bands contain the stiffness parameter of the  $\gamma$  oscillator [3, 8].

It often happens that a successful, but simple, model or approach spawns new generations of related approaches. This is especially the case if, despite its success, the data reveal certain, albeit perhaps small, discrepancies with the simple approach. A classic case of this is the simple formula for rotational spectra [1], which led to a myriad of alternate formulas (see for example Refs. [9, 10, 11, 12]), usually more and more parameters and, not surprisingly, working better. Of course, each such case ultimately entails a judgement as to whether the additional complications are worth the improved descriptions they yield.

The case of critical point symmetries is no exception. Despite their simplicity (square wells in  $\beta$  along with flat or harmonic oscillator potentials in the  $\gamma$  degree of freedom) and their success in describing transitional nuclei, it was immediately recognized that there were important discrepancies with the data as well. One, for example, occurs in X(5) where the predicted energy spacings in the excited  $0_2^+$  band are far too large [13, 14].

Since the advent of these CPS, a number of alternate geometrical models have been proposed and their predictions worked out. Some of these share with X(5) an extreme economy of parameters, others have one additional parameter. These models can all be solved exactly, either analytically or numerically. Some are, in fact, essentially identical to the CPS but are solved exactly, while others involve alternate, presumably more realistic potentials. One example, which we shall refer to occasionally, is the so-called Confined Beta Soft (CBS) model [15, 16] which takes as its starting point from X(5) but allows the inner wall to move out to the radius of the outer wall. As the inner wall moves, the spectra change smoothly from X(5) to a pure rotor. Other potentials [17, 18, 19], which we shall not consider, utilize triaxial shapes with non-zero values for the minimum of the potential in  $\gamma$ .

It is the purpose of this paper to explore a few of the most promising geometrical models, to compare their predictions with each other and with the data. We deal only with the

axially symmetric case at present, that is, nuclei whose potentials in  $\gamma$  are of harmonic oscillator type with a minimum at  $\gamma = 0^\circ$ .

These models can be grouped into three classes: one, called  $X_{\text{ex}}(5)$  is simply an exact numerical solution [20] of the Hamiltonian of  $X(5)$ , without the approximate separation of  $\beta$  and  $\gamma$  variables used in Ref. [3]. This type of exact solution has now become tractable, using the novel techniques introduced in Refs. [21, 22, 23]. It is worth mentioning that in  $X_{\text{ex}}(5)$ , the  $\gamma$  stiffness parameter is involved in all bands, while in  $X(5)$  the ground and  $\beta$  bands are independent of the  $\gamma$  stiffness parameter .

The other two classes each take advantage of a kind of potential that is exactly separable from the start. Such potentials have the form [4]

$$u_{ES}(\beta, \gamma) = u(\beta) + \frac{u(\gamma)}{\beta^2} \quad (1)$$

where ES stands for exactly separable. The first of these uses the same  $u(\beta)$  and  $u(\gamma)$  as  $X(5)$  itself - that is, the square well in  $\beta$  and a  $\gamma$  dependent potential given by a harmonic oscillator in  $\gamma$ . This is the so-called ES- $X(5)$  solution [24].

The second group of the exactly separable class of potentials uses the Davidson potential [25] in  $\beta$ , namely

$$u(\beta) = \beta^2 + \frac{\beta_0^4}{\beta^2} \quad (2)$$

where  $\beta_0$  is the free parameter and gives the position of the minimum of the potential in  $\beta$ . The use of the Davidson potential with an approximate separation of variables has been discussed in Refs. [26, 27]. In the present work, we examine the Davidson potential with an exactly separable potential, which we call exactly separable Davidson (ES-D). By including a harmonic oscillator potential in  $\gamma$ , analytic solutions can be derived in this form to describe well-deformed, axially symmetric nuclei. These Davidson potentials, along with the  $X(5)$  potential, are illustrated in Fig. 1(a) for both the approximate separation of variables (left) and the exactly separable cases (right). In Fig. 1(b), the Davidson potential in just the  $\beta$  degree of freedom is illustrated for a few values of the  $\beta_0$  parameter.

Before proceeding to a detailed discussion of the present solution of the Bohr Hamiltonian, it is useful to put the present work in a context of other solutions to the Bohr Hamiltonian. This Hamiltonian has been solved analytically in the  $\gamma$ -unstable case [ $u(\beta, \gamma) = u(\beta)$ ] using the Davidson potential of Eq. (2) as the  $\beta$ -potential [28], showing, that with increasing values of the  $\beta_0$  parameter, a transition from the spherical vibrator to a rigid non-spherical  $\gamma$ -unstable structure occurs. The link provided by  $O(5)$  between the  $\gamma$ -unstable geometrical model and the  $O(6)$  limit of the Interacting Boson Approximation (IBA) model [29] has also been previously studied [30]. Later, it was shown [31] that the above mentioned  $\gamma$ -unstable Bohr Hamiltonian with the Davidson potential is characterized by the symmetry  $SU(1,1) \times SO(5)$ , with  $SO(5)$  due to rotational invariance in the five-dimensional collective space, and with  $SU(1,1)$  due to the Davidson potential. If the potential is allowed to also depend on  $\gamma$ , no algebraic solution has been found, but it has been shown that numerical calculations converge much more rapidly in an  $SO(5)$  basis with  $\beta_0 \neq 0$  than in the usual spherical basis with  $\beta_0 = 0$  [21, 22, 23]: the relevant  $SO(5)$  spherical harmonics having

been calculated in Ref. [22]. The correspondence between this approach, called the algebraic collective model [23], and the different limiting symmetries of the Interacting Boson Approximation (IBA) model [29] has been studied in Refs. [32, 33]. This powerful method has been recently extended [34] to the  $SU(1,1) \times SO(N)$  case.

In view of the above, the present work is an analytic, special solution of the Bohr Hamiltonian with a Davidson  $\beta$ -potential appropriate for axially symmetric prolate deformed nuclei (since the  $\gamma$ -potential is taken to possess a steep minimum at  $\gamma = 0$ ), while the earlier solutions of Refs. [28, 31] refer to a Davidson  $\beta$ -potential in a  $\gamma$ -unstable framework. As a result, the present solution will turn out to be appropriate for the description of well-deformed axially symmetric nuclei, which comprise the bulk of well-deformed nuclei, while the solution of Refs. [28, 31] is appropriate for those  $\gamma$ -unstable nuclei between spherical and moderately deformed cases.

There are several advantages in the present ES-D solution which we will consider in detail. As mentioned above, no approximation is involved in the separation of variables. As a result, all bands (ground,  $\gamma$ , and  $\beta$ ) are treated on an equal footing depending on two parameters, the Davidson parameter  $\beta_0$  (which is the location of the minimum of the potential) and the stiffness  $c$  of the  $\gamma$  oscillator. Finally, the  $\beta^2$  term in the potential solves the spacing problem in the  $\beta$  band that plagues the infinite square well solutions. Of course, with a minimum in  $\gamma$  at  $0^\circ$  and a relatively steep potential in  $\gamma$ , the model is applicable only to axially deformed rotational nuclei.

Despite this constraint, it will be shown that the present solution provides good results for the spectra and  $B(E2)$  transition rates of almost all well deformed rare earth and actinide nuclei. Furthermore, it provides insights regarding the recently found correlation [35] between  $\gamma$  stiffness and the  $\gamma$ -bandhead energy, as well as the long standing problem of producing an Interacting Boson Approximation (IBA)  $SU(3)$  degenerate level scheme [29] within the framework of the Bohr Hamiltonian.

## 2 The ES-D model

Our starting point is the original Bohr Hamiltonian [1]

$$H = -\frac{\hbar^2}{2B} \left[ \frac{1}{\beta^4} \frac{\partial}{\partial \beta} \beta^4 \frac{\partial}{\partial \beta} + \frac{1}{\beta^2 \sin 3\gamma} \frac{\partial}{\partial \gamma} \sin 3\gamma \frac{\partial}{\partial \gamma} - \frac{1}{4\beta^2} \sum_{k=1,2,3} \frac{Q_k^2}{\sin^2\left(\gamma - \frac{2}{3}\pi k\right)} \right] + V(\beta, \gamma), \quad (3)$$

where  $\beta$  and  $\gamma$  are the usual collective coordinates, while  $Q_k$  ( $k = 1, 2, 3$ ) are the components of angular momentum in the intrinsic frame, and  $B$  is the mass parameter.

We assume that the reduced potential,  $u = 2BV/\hbar^2$ , can be separated into two terms of the form

$$u(\beta, \gamma) = u(\beta) + \frac{u(\gamma)}{\beta^2} \quad (4)$$

as in Refs. [4, 17, 18, 19] where the Schrödinger equation can then be separated exactly into two equations.

For the potential in  $\gamma$  we use a harmonic oscillator

$$u(\gamma) = (3c)^2\gamma^2 \quad (5)$$

and  $u(\beta)$  is taken as the Davidson potential [25, 28, 31]

$$u(\beta) = \beta^2 + \frac{\beta_0^4}{\beta^2}, \quad (6)$$

where  $\beta_0$  denotes the position of the minimum of the potential. As described in Appendix I, the resulting energy eigenvalues are given by

$$E_{n,L} = 2n + 1 + \sqrt{\frac{L(L+1) - K^2}{3} + \frac{9}{4} + \beta_0^4 + 3C(n_\gamma + 1)}, \quad n = 0, 1, 2, \dots \quad (7)$$

For  $K = 0$  one has  $L = 0, 2, 4, \dots$ , while for  $K \neq 0$  one obtains  $L = K, K + 1, K + 2, \dots$

Bands occurring in this solution, characterized by  $(n, n_\gamma)$ , include the ground state band  $(0, 0)$ , the  $\beta_1$ -band  $(1, 0)$ , the  $\gamma_1$ -band  $(0, 1)$ , and the first  $K = 4$  band  $(0, 2)$ . The relative position of all levels depends on the parameters  $\beta_0$  and  $C$ . ( $C = 2c$  is used in order to keep equations similar to those in Refs. [3] and [24].) All bands are treated on equal footing [36], in analogy with the SU(3) limit of the Interacting Boson Model [29].

Details on the calculation of  $B(E2)$  transition strengths are described in Appendix II. We note that the  $u(\gamma)$  potential used in the Bohr equation has to be periodic, because of coordinate symmetry constraints [1]. In Ref. [20] both the proper periodic potential  $(1 - \cos 3\gamma)$  and the approximate form  $\gamma^2$ , appropriate for small  $\gamma$ , have been used, yielding similar results. A more detailed study of this issue has been recently carried out [37], leading to the use of spheroidal or Mathieu functions. Periodic  $\gamma$ -potentials involving  $\cos 3\gamma$  have been used in an early solution involving a harmonic oscillator for the  $\beta$ -potential [38], as well as more recently in the framework of the algebraic collective model [21, 32, 33], where their treatment is tractable because  $\cos 3\gamma$  is, within a constant, an SO(5) spherical harmonic with  $v = 3$  and  $L = 0$  (where  $v$  the seniority and  $L$  the angular momentum) [21]. The potential  $\csc^2 3\gamma$ , which is the partner of the infinite well potential in supersymmetric quantum mechanics [39], has also been used recently [40] in the Bohr Hamiltonian for triaxial nuclei. It is certainly of interest to examine the consequences of the use of periodic  $\gamma$  potentials in the present approach in subsequent work.

In the present paper we are going to follow Ref. [8], normalizing  $\Delta K = 0$  transitions to  $2_1^+ \rightarrow 0_1^+$ , and  $\Delta K = 2$  transitions to  $2_\gamma^+ \rightarrow 0_1^+$ . In this way normalization difficulties vanish.

The spectrum and  $B(E2)$  transition strengths of ES-X(5) are described for completeness in Appendix III.

## 3 Numerical results and comparison to experiment

### 3.1 Energy ratios

In Fig. 2(a), the  $R_{4/2} = E(4_1^+)/E(2_1^+)$  ratio as a function of the parameter  $C$  is shown for the ES-D solution (for a few values of the Davidson parameter  $\beta_0$ ) and ES-X(5), as well

as for the exact numerical solution  $[X_{\text{ex}}(5)]$  of Ref. [20]. The parameter  $C$  is connected to the parameter  $a$  of the exact numerical solution [20] through  $C = \frac{2}{3}\sqrt{a}$ . In Figs. 2(b) and (c), the ratios  $R_{0/2} = E(0_{\beta}^+)/E(2_1^+)$  and  $R_{2/2} = E(2_{\gamma}^+)/E(2_1^+)$ , corresponding to the normalized  $\beta$  and  $\gamma$  bandhead energies, respectively, are shown for the same solutions. The ES-D solution with  $\beta_0 = 0$  corresponds to the ES-X(5)- $\beta^2$  solution of Ref. [24].

From Fig. 2(a), it is clear that the ES-D and ES-X(5) solutions are appropriate mostly for well-deformed nuclei, while the exact numerical solution [20] is also applicable to less deformed nuclei (including the  $a = 200$  case [ $C = 9.428$ ] which gives results similar to the original X(5) model [3]). This difference is due to the  $\beta^2$  term in the potential  $u(\beta)+u(\gamma)/\beta^2$  used in the exactly separable cases. Within the ES-D solution, the rotational limit of  $R_{4/2} = 10/3$  is closely approached already for  $\beta_0 = 4$ .

As seen in Fig. 2(b), the normalized  $\beta$  bandhead energy,  $R_{0/2}$ , has a large dependence on the parameter  $\beta_0$  and shows less variation with the stiffness parameter  $C$ , particularly for large  $\beta_0$  values. This dependence is reversed for the normalized  $\gamma$  bandhead energy,  $R_{2/2}$ , which varies only slightly for different  $\beta_0$  values, but has a large dependence on the  $C$  parameter. As a result, the  $R_{2/2}$  and  $R_{0/2}$  lines cross in ES-D at values of  $C$  increasing with  $\beta_0$ . These lines also cross in the numerical solution [20], but they do not cross in ES-X(5). This point will be further discussed in the next subsection.

Concerning the results of the exact numerical solution  $X_{\text{ex}}(5)$  of Ref. [20] used for comparisons in this and in subsequent sections, our assignment of levels to a particular band follows the same as given in Ref. [20]. In particular,  $2_{\gamma}^+$  corresponds to  $2_2^+$  for  $a = 0 - 450$  and to  $2_3^+$  for  $a = 500 - 1000$ , while  $2_{\beta}^+$  corresponds to  $2_3^+$  for  $a = 0 - 450$  and to  $2_2^+$  for  $a = 500 - 1000$ . Similarly,  $4_{\gamma}^+$  corresponds to  $4_2^+$  for  $a = 0 - 650$  and to  $4_3^+$  for  $a = 700 - 1000$ , while  $4_{\beta}^+$  corresponds to  $4_3^+$  for  $a = 0 - 650$  and to  $4_2^+$  for  $a = 700 - 1000$ . These assignments are related to avoided crossings, as explained in Ref. [20].

### 3.2 Relative spacings within different bands and relative positions of bandheads

In Fig. 3(a) the energy ratio

$$R_{2\beta} = \frac{E(2_{\beta}^+) - E(0_{\beta}^+)}{E(2_1^+)} \quad (8)$$

is shown for the solutions under discussion. The ratio is exactly 1 in the case of ES-D, irrespective of the value of the Davidson parameter  $\beta_0$ . This is due to the oscillator term in the Davidson potential which gives equal rotational spacings in the ground state band and the  $\beta$  band. Thus, the same holds for the energy ratio

$$R_{4\beta} = \frac{E(4_{\beta}^+) - E(2_{\beta}^+)}{E(4_1^+) - E(2_1^+)}, \quad (9)$$

shown in Fig. 3(b). In Fig. 3(c) the energy ratio

$$R_{\gamma} = \frac{E(4_{\gamma}^+) - E(2_{\gamma}^+)}{E(4_1^+) - E(2_1^+)} \quad (10)$$

is shown, while in Fig. 3(d) the energy ratio

$$R_{\beta\gamma} = R_{0/2} - R_{2/2} = \frac{E(0_{\beta}^{+}) - E(2_{\gamma}^{+})}{E(2_{1}^{+})} \quad (11)$$

is given. Abrupt changes in the predictions of  $X_{\text{ex}}(5)$  are due to the avoided crossings of  $(2_{2}^{+}, 2_{3}^{+})$  and  $(4_{2}^{+}, 4_{3}^{+})$ .

Experimental data for the energy ratios shown in Fig. 3 are exhibited in Fig. 4. Since the current solution is only applicable to well-deformed nuclei, the data included in Fig. 4 is limited to  $A > 100$  and  $R_{4/2} > 3.00$ . Comparing Figs. 3(a) and 4(a) we see that in terms of the energy ratio  $R_{2\beta}$ , which compares the level spacing within the  $\beta$  band to the level spacing within the ground state band, most nuclei exhibit a ratio slightly less than 1.0. This feature is most closely reproduced by the ES-D solution which predicts a ratio of exactly 1.0, independent of the value of the Davidson parameter  $\beta_0$ . The predictions of the ES-X(5) solution for  $R_{2\beta}$  are higher by 50% or more, and the predictions of  $X_{\text{ex}}(5)$  are even higher. (This is the well known problem of overprediction of the spacing of the  $\beta$  band in the X(5) model by a factor close to two [13, 14], which can be resolved by replacing the infinite well potential by a potential with linear sloped walls [41].) The same is seen for the energy ratio  $R_{4\beta}$  in Figs. 3(b) and 4(b).

From Fig. 4(c), it is clear that the majority of the data for the energy ratio  $R_{\gamma}$ , which compares the level spacing within the  $\gamma$  band to the level spacing within the ground state band, is centered around values of 1.0. The predictions for  $R_{\gamma}$  from each of the solutions overlap and are consistent with the range observed in the data. The ES-D solution gives the largest range of predictions, since this is a more flexible model (2 parameters) compared with the single parameter  $X_{\text{ex}}(5)$  and ES-X(5) solutions. Overall, all three solutions yield reasonable predictions for the  $\gamma$ -band spacings in deformed nuclei.

The experimental energy ratio  $R_{\beta\gamma}$ , which is related to the relative positioning of the  $\beta$  and  $\gamma$  bandhead energies, exhibits a wide range of values spanning positive to negative, as shown in Fig. 4(d). As a result, we expect that the solutions exhibiting both positive and negative values for this ratio, namely the ES-D solution for not very high values of the Davidson parameter  $\beta_0$  and  $X_{\text{ex}}(5)$ , should better reproduce this feature.

Summarizing the above observations, all three solutions under consideration, ES-D, ES-X(5) and  $X_{\text{ex}}(5)$ , are found to give reasonable predictions for the  $\gamma$ -band spacing, while the ES-D solution yields predictions which most closely reproduce the  $\beta$ -band spacing of most deformed nuclei. The ES-D solution (for not very high values of the parameter  $\beta_0$ ) and the  $X_{\text{ex}}(5)$  solution appear to reproduce the relative positions of the  $\beta$  and  $\gamma$  bandhead energies in a number of nuclei. Thus, the ES-D solution provides the flexibility to describe a wide range of observables (spacings within the  $\beta$  and  $\gamma$  bands, relative position of the  $\beta$  and  $\gamma$  bandheads) with not very large values of the Davidson parameter  $\beta_0$ .

### 3.3 $B(E2)$ ratios

Having examined the main features of the energy spectra, we turn now to the study of the characteristics of the  $B(E2)$  transition rates. As mentioned in Sec. 2, in order to avoid normalization problems,  $\Delta K = 0$  transitions will be normalized to the  $2_{1}^{+} \rightarrow 0_{1}^{+}$  transition, while  $\Delta K = 2$  transitions will be normalized to the  $2_{\gamma}^{+} \rightarrow 0_{1}^{+}$  transition, as in Ref. [8].

We include in this comparison the predictions of the original X(5) solution as well as the U(5) and SU(3) limits of the IBA. X(5) predictions for ground  $\rightarrow$  ground,  $\beta \rightarrow \beta$ , and  $\beta \rightarrow$  ground transitions are taken from Ref. [3], while X(5) predictions for  $\gamma \rightarrow \gamma$ ,  $\gamma \rightarrow$  ground, and  $\gamma \rightarrow \beta$  transitions are taken from Ref. [8]. SU(3) predictions for the ground  $\rightarrow$  ground and  $\beta \rightarrow \beta$  transitions are obtained with the standard quadrupole operator of the IBA [29], while predictions for  $\beta \rightarrow$  ground and  $\gamma \rightarrow$  ground transitions are obtained with the extended quadrupole operator containing the extra term  $(d^\dagger \times \tilde{s} + s^\dagger \times \tilde{d})^{(2)}$  [29].

Intraband transitions within the ground state and  $\beta$  band are shown in Fig. 5. Within the ground state band, Fig. 5(a), the ES-D predictions lie in between X(5) and SU(3) for most values of  $C$ . Again, for  $\beta_0$  values of 4 and larger, the SU(3) limit is almost exactly achieved. For the transitions within the  $\beta$  band, shown in Figs. 5(b),(c), the ES-D predictions lie between U(5) and SU(3), approaching the latter with increasing values of  $\beta_0$ . In the case of the ratio  $B(E2; 2_\beta^+ \rightarrow 0_\beta^+) / B(E2; 2_1^+ \rightarrow 0_1^+)$ , the X(5) predictions lie below the SU(3) value, and not between the U(5) and SU(3) values, as might have been expected, since they are related to the transition between U(5) and SU(3). As with the energy spectra, the  $\beta$  band predictions again exhibit the largest differences between ES-D and X(5).

Transitions from the  $\gamma$  band are shown in Fig. 6. The ES-D predictions are consistently close to X(5) or intermediate between X(5) and the SU(3) limit. This is particularly true for the branching ratios from the  $\gamma$  band given in Figs. 6(b),(c).

The  $\beta$  band to ground band transitions are shown in Fig. 7. For the transition from the  $0_2^+$  state to the ground state  $2_1^+$ , the predictions of ES-D are intermediate between X(5) and SU(3) for most values of  $C$ . The decay from the  $2_\beta^+$  state to the ground state band, Figs. 7(b),(c), shows some variation between the models, but all are similar in magnitude. These small differences become more evident when branching ratios are considered, as in Fig. 7(d). For the ratio,  $B(E2; 2_\beta^+ \rightarrow 4_1^+) / B(E2; 2_\beta^+ \rightarrow 0_1^+)$ , the X(5) predictions are nearly an order of magnitude larger than the SU(3) ratio (also the Alaga ratio) of 2.6. The ES-D predictions are again intermediate between X(5) and SU(3).

The  $\gamma$  band to  $\beta$  band transitions are shown in Fig. 8. The predictions of ES-D for growing  $\beta_0$  approach X(5).

In summary, in (almost) all cases the ES-D predictions lie in general between the X(5) and SU(3) predictions, with SU(3) already approached at  $\beta_0 = 4$ .

### 3.4 Fits to specific nuclei

A search has been made to find nuclei for which the ground state,  $\beta$ , and  $\gamma$  bands (up to the point of backbending or upbending in each band) can be well reproduced by the ES-D solution. Since the ES-D solution is appropriate only for deformed nuclei, the search was constrained to nuclei with  $R_{4/2} > 3.00$ . Considering all such nuclei in the rare-earth and actinide regions, we find that almost all nuclei with a known  $0_2^+$  and  $2_\gamma^+$  state can be well described in terms of energies by ES-D, as shown in Table 1. The quality measure

$$\sigma = \sqrt{\frac{\sum_{i=1}^n (E_i(exp) - E_i(th))^2}{(n-1)E(2_1^+)}} \quad (12)$$

used for evaluating the rms fits performed, remains less than one in most cases. Out of the  $\sim 60$  nuclei which meet the above criteria, there are only two cases where the ES-D solution does not provide a good description of all the bandhead energies, namely  $^{152}\text{Sm}$  and  $^{154}\text{Gd}$ . These exceptions are not surprising, since these nuclei are well described by the X(5) model, which uses a “flat-bottomed” potential in the  $\beta$  degree of freedom. The ES-D solution, on the other hand, incorporates a potential which is much “stiffer” in the  $\beta$  degree of freedom. Thus, discrepancies between the data and the ES-D solution are expected in transitional nuclei and, indeed, may be used to point to nuclei with flat potentials in the  $\beta$  degree of freedom.

Several  $B(E2)$  ratios obtained with ES-D using the same parameters as given in Table 1 are shown in Table 2, which includes all nuclei of Table 1 for which nontrivial information on relevant  $B(E2)$ s is experimentally known [45]. More detailed level schemes for  $^{156}\text{Gd}$  and  $^{232}\text{Th}$  are shown in Fig. 9, as examples of the quality of the ES-D solution to reproduce detailed spectra.

As seen in Table 2, the intraband  $B(E2)$  ratios within the ground state bands are reproduced quite well for a majority of the nuclei, despite the fact that  $B(E2)$  values have not been taken into account in the fitting procedure. Also, the theoretical  $\gamma \rightarrow$  ground  $B(E2)$  ratios are in very good agreement with the experiment values. However, the theoretical  $\gamma \rightarrow$  ground  $B(E2)$  strengths, when normalized to the  $2_1^+ \rightarrow 0_1^+$  transition, are much lower than the experimental ones. This could be due to the normalization difficulties mentioned at the end of Sec. 2, which disappear if ratios of  $\gamma \rightarrow$  ground transitions are used. Moreover, the theoretical interband  $\beta \rightarrow$  ground  $B(E2)$  values are consistently an order of magnitude higher than the experimental values.

### 3.5 Bandheads

The ability of the present model to reproduce the general experimental trends of  $R_{0/2} = E(0_\beta^+)/E(2_1^+)$  and of  $R_{2/2} = E(2_\gamma^+)/E(2_1^+)$  as a function of  $R_{4/2} = E(4_1^+)/E(2_1^+)$  is shown in Figs. 10(a),(b). Predictions of the ES-X(5), Confined Beta Soft (CBS) [15, 16] and  $X_{\text{ex}}(5)$  solutions are also shown for comparison. From Eq. (7) it is clear that the energy levels of the ground state and  $\beta$  bands depend only on the parameter combination  $\beta_0^4 + 3C$ , thus in Fig. 10(a) only one curve appears for ES-D, with  $\beta_0^4 + 3C$  increasing from left to right. From the same equation it is also clear that the levels of the  $\gamma$  band depend on the parameter combination  $\beta_0^4 + 6C$ . As a result, different curves are obtained for ES-D in Fig. 10(b) by fixing  $\beta_0$  to different values and varying the  $C$  parameter.

The predictions for  $R_{0/2}$  as a function of  $R_{4/2}$  are more less the same for the ES-D, ES-X(5) and CBS solutions. The  $X_{\text{ex}}(5)$  predictions for  $R_{0/2}$  are slightly higher and above the overall trend of the data.

As discussed previously, in the CBS solution and other X(5)-related solutions, the bandhead energy of the  $\gamma$  band depends on a free parameter. In the present exactly separable (ES) solutions, it is treated on an equal footing as the  $\beta$  bandhead energy. The plot of  $R_{2/2}$  vs.  $R_{4/2}$  reveals that a large set of data corresponds to the ES-D region with  $\beta_0$  between 2 and 4. The same set is also described quite well by the ES-X(5) curve. Figure 10(b) also reveals that the predictions of the ES-D solution for the  $\gamma$  bandhead energy are only in agreement with the data for  $R_{4/2}$  values larger than 3.0. This is again related to the present

solution being applicable only to axially symmetric well-deformed nuclei, since when the parameter  $C$  becomes too small, the approximation of an axially symmetric potential is no longer valid. On the other hand,  $X_{\text{ex}}(5)$  provides a better description of  $R_{2/2}$  for  $R_{4/2}$  values between 2.6 and 3.0.

### 3.6 Gamma-stiffness

In Ref. [35] a correlation has been found between the gamma stiffness of the potential and the ratio  $R_{2/2} = E(2_{\gamma}^+)/E(2_1^+)$ , with the gamma-stiffness increasing stronger than linearly as a function of  $R_{2/2}$ . In the present model, the gamma-stiffness coefficient  $(3c)^2$  is shown as a function of  $R_{2/2}$  in Fig. 11(a). It is evident that a stronger than linear increase is seen, which varies little with  $\beta_0$ , at least for reasonable values of the latter, as indicated from Table 1. The specific points corresponding to the rare earth and actinide nuclei of Table 1 are shown in Fig. 11(b), exhibiting the same trend.

A short discussion is now in place on the qualitative correspondence between the two parameters ( $\beta_0$ ,  $C$ ) of the present solution and those of the usual two-parameter IBA-1 Hamiltonian [46, 47]

$$H(\zeta, \chi) = C \left[ (1 - \zeta) \hat{n}_d - \frac{\zeta}{4N_B} \hat{Q}^x \cdot \hat{Q}^x \right], \quad (13)$$

where  $\hat{n}_d = d^\dagger \cdot \tilde{d}$ ,  $\hat{Q}^x = (s^\dagger \tilde{d} + d^\dagger s) + \chi (d^\dagger \tilde{d})^{(2)}$ ,  $N_B$  is the number of valence bosons, and  $C$  is a scaling factor. The above Hamiltonian contains two parameters,  $\zeta$  and  $\chi$ , with the parameter  $\zeta$  ranging from 0 to 1, and the parameter  $\chi$  ranging from 0 to  $-\sqrt{7}/2 = -1.32$ . The IBA dynamical symmetries are given by  $\zeta = 0$ , any  $\chi$  for U(5),  $\zeta = 1$ ,  $\chi = -\sqrt{7}/2$  for SU(3), and  $\zeta = 1$ ,  $\chi = 0$  for O(6). As remarked in Ref. [35], stiffness is proportional to the IBA parameter  $\chi$ . Thus, in the present case  $(3c)^2$  roughly corresponds to  $|\chi|$ . On the other hand, we have already seen that increasing  $\beta_0$  leads to the SU(3) limit, thus  $\beta_0$  is in qualitative correspondence to  $\zeta$ . It should be emphasized, however, that while the IBA Hamiltonian of Eq. (13) can cover the whole region from U(5) ( $R_{4/2} = 2$ ) to SU(3) ( $R_{4/2} = 3.33$ ), the ES-D solution provides reasonable results only in the narrow region of  $R_{4/2}$  between 3.0 and 3.33.

### 3.7 Occurrence of SU(3) degeneracy

A long standing problem has been deriving from the Bohr Hamiltonian a spectrum similar to that of the SU(3) limit of the Interacting Boson Approximation (IBA) model [29]. The main features of the spectrum should be:

- a) The energy spacings among the  $2^+$ ,  $4^+$ ,  $6^+$ , ... levels within the ground,  $\beta$  and  $\gamma$  bands should be identical.
- b) Furthermore, the  $2^+$ ,  $4^+$ ,  $6^+$ , ... levels of the  $\beta$  and  $\gamma$  bands should be degenerate.

In the present model, the spacings within the ground and  $\beta$  bands are identical, because of the oscillator term in the  $u(\beta)$  potential, as already seen in subsection 3.2. It is therefore sufficient to examine the conditions under which the  $2^+$ ,  $4^+$ ,  $6^+$ , ... levels of the  $\beta$  and  $\gamma$  bands are degenerate.

From Eq. (7) it is trivial to see that the energy spacings in the  $\beta$  and  $\gamma$  bands become equal for any  $L$  if  $C = 4/9$  (since in this case the  $3C$  term in the  $\beta$  band is counterbalanced by the  $-K^2/3 + 6C$  term in the  $\gamma$  band, which has  $K = 2$ ). However, this observation is of little physical significance, since the values of  $C$  appropriate for actual nuclei, appearing in Table 1, are considerably higher.

Figs. 3(b), (c) indicate that in general the spacings within the  $\gamma$  band are lower than the spacings within the  $\beta$  band by about 20% for most  $\beta_0$  and  $C$  values of interest. Thus within the present solution one can only hope to reproduce a situation with approximate degeneracy for the first few even levels of the  $\beta$  and  $\gamma$  bands.

From Eq. (7), the requirement  $E(2_\beta^+) = E(2_\gamma^+)$  leads to the condition  $9C^2 - 80C - 16\beta_0^4 - 356/9 = 0$ , while the requirement  $E(4_\beta^+) = E(4_\gamma^+)$  leads to the condition  $9C^2 - 80C - 16\beta_0^4 - 1028/9 = 0$ . Similar conditions occur from the requirement  $E(L_\beta^+) = E(L_\gamma^+)$  for higher  $L$ . These conditions can be approximately satisfied simultaneously only for very large values of  $\beta_0$ , which are outside the region of physical interest according to the  $\beta_0$  values appearing in Table 1, since too high  $\beta_0$  would result in too high a  $0_\beta^+$  bandhead energy.

In this way one is led to consider what happens for a fixed value of  $R_{0/2} = E(0_\beta^+)/E(2_1^+)$ . In this case Eq. (7) easily leads to

$$3C = \left( \frac{R_{0/2}}{2} - \frac{1}{R_{0/2}} \right)^2 - \beta_0^4 - \frac{9}{4}. \quad (14)$$

Thus for a given  $R_{0/2}$  one can minimize with respect to  $\beta_0$  the rms deviation between the even levels of the  $\beta$  and  $\gamma$  bands

$$\sigma_{\beta,\gamma}(L_{max}) = \sqrt{\frac{1}{L_{max}/2 - 1} \sum_{L=2}^{L_{max}} \left( \frac{E(L_\beta^+) - E(L_\gamma^+)}{E(2_1^+)} \right)^2}, \quad (15)$$

the value of  $C$  obtained for each  $\beta_0$  from Eq. (15). Numerical results shown in Table 3 indicate that a reasonable degree of degeneracy is obtained for  $L_{max} = 10$  and  $R_{0/2} \geq 15$ , which is of physical interest, since the  $R_{0/2}$  values in Table 1 extend up to 27. In Table 4, the results of the fit to  $^{232}\text{Th}$ , corresponding to the values reported in Table 1 are given. In the case of  $^{232}\text{Th}$ , which is very close to the  $R_{0/2} = 15$  case reported in Table 3, one can see that  $\sigma_{\beta,\gamma}^{th}(L_{max} = 10) = 1.142$ , while  $\sigma_{\beta,\gamma}^{exp}(L_{max} = 10) = 0.593$ . Therefore, although the overall fit is quite good, the degree of degeneracy obtained from theory is less than the one indicated by experiment. One could conclude that the present solution does contain parameter pairs which correspond to an approximate degeneracy of the low-lying even levels of the  $\beta$  and  $\gamma$  bands, while at the same time the spacings within the  $\beta$  band are identical to the spacings within the ground band, however the problem of reproducing a SU(3) spectrum from the Bohr Hamiltonian remains conceptually open.

### 3.8 Alhassid-Whelan arc of regularity

It has been recently suggested that an experimental confirmation [48] of the Alhassid-Whelan arc of regularity [49], connecting the U(5) and SU(3) symmetries in the symmetry triangle [50] of the Interacting Boson Approximation (IBA) model [29] is manifested in nuclei in which the  $\beta$  and  $\gamma$  bandheads,  $0_\beta^+$  and  $2_\gamma^+$ , are nearly degenerate.

From Eq. (7) the requirement  $E(0_\beta^+) = E(2_\gamma^+)$  leads to the condition  $9C^2 - 68C - 16\beta_0^4 - 224/9 = 0$ . Given the fact that  $C$  has to be nonnegative, this condition leads to  $C = (34 + \sqrt{1380 + 144\beta_0^4})/9$ . Among the nuclei listed in Table 1, the ones satisfying the condition  $|E(2_\gamma^+) - E(0_\beta^+)|/E(2_\gamma^+) \leq 0.05$  [48] are  $^{158}\text{Gd}$ ,  $^{158}\text{Dy}$ ,  $^{170}\text{Er}$ ,  $^{178}\text{Hf}$ ,  $^{236}\text{U}$ , and  $^{248}\text{Cm}$ .

From the  $\beta_0$  and  $C$  values listed in Table 1, one can see that the above condition is closely fulfilled. However, since the ES-D solution is applicable mostly to nuclei with  $R_{4/2} \geq 3.0$ , the above mentioned condition describes only a small part of the arc of regularity close to the SU(3) limit.

## 4 Conclusions

In the present paper, an exactly separable version of the Bohr Hamiltonian, called ES-D, which uses a potential of the form  $u(\beta) + u(\gamma)/\beta^2$ , with a Davidson potential  $\beta^2 + \beta_0^4/\beta^2$  in the place of  $u(\beta)$ , and a harmonic oscillator with a minimum at  $\gamma = 0^\circ$  as  $u(\gamma)$ , is developed. All bands (e.g., ground,  $\beta$  and  $\gamma$ ) in this solution are treated on an equal footing, depending on two parameters, the Davidson parameter  $\beta_0$  and the stiffness  $c$  of the  $\gamma$ -potential. The solution is found to be applicable only to well deformed nuclei (with  $R_{4/2} \geq 3.0$ ) due to the  $\beta^2$  denominator in the  $u(\gamma)$  term. Nevertheless, it reproduces very well the bandheads and energy spacings within bands of almost all rare earth and actinide nuclei, with  $R_{4/2} \geq 3.0$ , for which available data exists, as well as most of the inter-ground and intra- $\gamma$  band  $B(E2)$  transition rates. The most glaring discrepancy concerns  $B(E2)$  values for the  $\beta$  band to ground band transitions which are typically overpredicted by an order of magnitude. The two exceptions where ES-D does not provide a good description of energy spectra are  $^{152}\text{Sm}$  and  $^{154}\text{Gd}$ , which have previously been shown to be well reproduced with the infinite square well potential of the critical point symmetry X(5). Furthermore, the ES-D solution provides insights regarding the recently found correlation between the  $\gamma$  stiffness and the  $\gamma$ -bandhead energy, as well as the long standing problem of producing a level scheme with IBA SU(3) degeneracies within the framework of the Bohr Hamiltonian.

However, several open questions remain, in particular, concerning the discrepancies in the  $B(E2)$  predictions. The underprediction of the  $\gamma \rightarrow$  ground and  $\gamma \rightarrow \beta$   $B(E2)$ s can be attributed to two reasons. First, the  $\beta^2$  denominator in the  $u(\gamma)$  term, “pushes” the nucleus to more rigid axial behavior. This can be investigated through a detailed comparison of  $B(E2)$ s predicted by ES-X(5) and the exact numerical solution of Ref. [20], since the same  $u(\beta)$  and  $u(\gamma)$  potentials are used in both cases. Work in this direction is in progress. The second reason is the use of a harmonic oscillator potential for  $u(\gamma)$ , as an approximation valid for small  $\gamma$ , instead of a potential periodic in  $\gamma$ . This can be studied through the use of a periodic  $\gamma$  potential [37] in ES-D, since no approximations will be present in this case.

Furthermore, an exact numerical solution parallel to Ref. [20] utilizing a  $u(\beta) + u(\gamma)/\beta^2$  potential with a Davidson potential as  $u(\beta)$  should demonstrate the degree of importance of  $\beta$ - $\gamma$  coupling when compared to the present results.

## Acknowledgements

Valuable discussions with F. Iachello, R.V. Jolos and M.A. Caprio are acknowledged. This work was supported by U.S. DOE Grant No. DE-FG02-91ER-40609.

## Appendix I: Spectrum of ES-D

One seeks [3] solutions of the relevant Schrödinger equation having the form  $\Psi(\beta, \gamma, \theta_i) = \phi_K^L(\beta, \gamma) \mathcal{D}_{M,K}^L(\theta_i)$ , where  $\theta_i$  ( $i = 1, 2, 3$ ) are the Euler angles,  $\mathcal{D}(\theta_i)$  denote Wigner functions of them,  $L$  are the eigenvalues of angular momentum, while  $M$  and  $K$  are the eigenvalues of the projections of angular momentum on the laboratory-fixed  $z$ -axis and the body-fixed  $z'$ -axis respectively.

As pointed out in Ref. [3], in the case in which the potential has a minimum around  $\gamma = 0$  one can write the angular momentum term of Eq. (3) in the form

$$\sum_{k=1,2,3} \frac{Q_k^2}{\sin^2\left(\gamma - \frac{2\pi}{3}k\right)} \approx \frac{4}{3}(Q_1^2 + Q_2^2 + Q_3^2) + Q_3^2 \left( \frac{1}{\sin^2\gamma} - \frac{4}{3} \right). \quad (16)$$

Using this result in the Schrödinger equation corresponding to the Hamiltonian of Eq. (3), introducing [3] reduced energies  $\epsilon = 2BE/\hbar^2$  and reduced potentials  $u = 2BV/\hbar^2$ , and assuming that the reduced potential can be separated into two terms of the form  $u(\beta, \gamma) = u(\beta) + u(\gamma)/\beta^2$ , as in Refs. [4, 17, 18, 19], the Schrödinger equation can be separated into two equations

$$\left[ -\frac{1}{\beta^4} \frac{\partial}{\partial \beta} \beta^4 \frac{\partial}{\partial \beta} + \frac{L(L+1)}{3\beta^2} + u(\beta) + \frac{\lambda}{\beta^2} \right] \xi_L(\beta) = \epsilon \xi_L(\beta), \quad (17)$$

$$\left[ -\frac{1}{\sin 3\gamma} \frac{\partial}{\partial \gamma} \sin 3\gamma \frac{\partial}{\partial \gamma} + \frac{K^2}{4} \left( \frac{1}{\sin^2\gamma} - \frac{4}{3} \right) + u(\gamma) \right] \eta_K(\gamma) = \lambda \eta_K(\gamma). \quad (18)$$

Eq. (18) for  $\gamma \approx 0$  can be treated as in Ref. [3], considering a potential of the form  $u(\gamma) = (3c)^2 \gamma^2$  and expanding in powers of  $\gamma$ . Then Eq. (18) takes the form

$$\left[ -\frac{1}{\gamma} \frac{\partial}{\partial \gamma} \gamma \frac{\partial}{\partial \gamma} + \frac{K^2}{4\gamma^2} + (3c)^2 \gamma^2 \right] \eta_K(\gamma) = \epsilon_\gamma \eta_K(\gamma), \quad (19)$$

with  $\epsilon_\gamma = \lambda + \frac{K^2}{3}$ . The solution is given in terms of Laguerre polynomials [3]

$$\epsilon_\gamma = (3C)(n_\gamma + 1), \quad C = 2c, \quad n_\gamma = 0, 1, 2, \dots, \quad (20)$$

$$n_\gamma = 0, \quad K = 0; \quad n_\gamma = 1, \quad K = \pm 2; \quad n_\gamma = 2, \quad K = 0, \pm 4; \quad \dots, \quad (21)$$

$$\eta_{n_\gamma, |K|}(\gamma) = C_{n_\gamma, |K|} \gamma^{|K/2|} e^{-(3c)\gamma^2/2} L_{\tilde{n}}^{|K/2|}(3c\gamma^2), \quad \tilde{n} = (n_\gamma - |K/2|)/2. \quad (22)$$

Eq. (17) is then solved exactly for the case in which  $u(\beta)$  is a Davidson potential [25, 28, 31]

$$u(\beta) = \beta^2 + \frac{\beta_0^4}{\beta^2}, \quad (23)$$

where  $\beta_0$  denotes the position of the minimum of the potential. In this case the eigenfunctions are [42]

$$F_n^L(\beta) = \left[ \frac{2n!}{\Gamma\left(n + a + \frac{5}{2}\right)} \right]^{1/2} \beta^a L_n^{a+\frac{3}{2}}(\beta^2) e^{-\beta^2/2}, \quad (24)$$

where  $\Gamma(n)$  stands for the  $\Gamma$ -function,  $L_n^a(z)$  denotes the Laguerre polynomials, and

$$a = -\frac{3}{2} + \sqrt{\frac{L(L+1) - K^2}{3} + \frac{9}{4} + \beta_0^4 + 3C(n_\gamma + 1)}, \quad (25)$$

while the energy eigenvalues are

$$E_{n,L} = 2n + a + \frac{5}{2} = 2n + 1 + \sqrt{\frac{L(L+1) - K^2}{3} + \frac{9}{4} + \beta_0^4 + 3C(n_\gamma + 1)}, \quad n = 0, 1, 2, \dots \quad (26)$$

For  $K = 0$  one has  $L = 0, 2, 4, \dots$ , while for  $K \neq 0$  one obtains  $L = K, K + 1, K + 2, \dots$

In the above,  $n$  is the usual oscillator quantum number. A formal correspondence between the energy levels of X(5) and the present solution can be established through the relation

$$n = s - 1. \quad (27)$$

It should be remembered, however, that the origin of the two quantum numbers is different,  $s$  labelling the order of a zero of a Bessel function and  $n$  labelling the number of zeros of a Laguerre polynomial. In the present notation, the ground state band corresponds to  $n = 0$  ( $s = 1$ ). For the energy states the notation  $E_{s,L} = E_{n+1,L}$  of Ref. [3] will be kept.

The full wave function reads

$$\Psi(\beta, \gamma, \theta_i) = F_n^L(\beta) \eta_{n_\gamma, |K|}(\gamma) \mathcal{D}_{MK}^L(\theta_i), \quad (28)$$

and should be properly symmetrized [43]

$$\Psi(\beta, \gamma, \theta_i) = F_n^L(\beta) \eta_{n_\gamma, |K|}(\gamma) \sqrt{\frac{2L+1}{16\pi^2(1+\delta_{K,0})}} \left( \mathcal{D}_{M,K}^L + (-1)^L \mathcal{D}_{M,-K}^L \right). \quad (29)$$

It should be noticed at this point that Eq. (17) for  $\lambda = 0$  takes the form appearing in the framework of a X(5) solution with the infinite well potential replaced by a Davidson potential, called X(5)-D in the usual terminology. From the expression for  $\lambda$  given below Eq. (19) it is clear that  $\lambda = 0$  is achieved for  $K = 0$  and  $\epsilon_\gamma = 0$ , i.e.  $C = 0$ . It is therefore proved that the numerical results of the ES-D solution for the  $K = 0$  bands (ground state band and beta bands) will coincide with the corresponding results of X(5)-D. This result should be considered as a numerical coincidence, because  $C = 0$  is not acceptable in the framework of ES-D, since the approximation of  $\gamma$  being close to zero collapses in this case. The lowest  $R_{4/2}$  value within the present model is obtained for  $\beta_0 = 0$  and  $C = 0$ , which corresponds to the X(5)- $\beta^2$  solution [51], giving  $R_{4/2} = 2.646$ . Thus, while  $\beta_0$  suggests a spherical shape, the contribution from centrifugal term in the potential results in a non-zero value for the average deformation.

## Appendix II: $B(E2)$ values of ES-D

B(E2) transition rates

$$B(E2; LK \rightarrow L'K') = \frac{5}{16\pi} \frac{|\langle L'K' || T^{(E2)} || LK \rangle|^2}{2L+1} \quad (30)$$

can be calculated using the quadrupole operator [3]

$$T^{(E2)} = t\beta \left[ \mathcal{D}_{\mu,0}^{(2)} \cos \gamma + \frac{1}{\sqrt{2}} (\mathcal{D}_{\mu,2}^{(2)} + \mathcal{D}_{\mu,-2}^{(2)}) \sin \gamma \right], \quad (31)$$

where  $t$  is a scale factor, and the Wigner-Eckart theorem in the form

$$\langle L'M'K'|T_{\mu}^{(E2)}|LMK\rangle = \frac{1}{\sqrt{2L'+1}} \langle L2L'|M\mu M'\rangle \langle L'K' || T^{(E2)} || LK\rangle. \quad (32)$$

In ground  $\rightarrow$  ground,  $\beta \rightarrow$  ground,  $\beta \rightarrow \beta$  and  $\gamma \rightarrow \gamma$  transitions, only the first term of Eq. (31) contributes, since the relevant angular momentum coupling coefficients involving the second term vanish, while in  $\gamma \rightarrow$  ground and  $\gamma \rightarrow \beta$  transitions only the second term of Eq. (31) contributes, since the relevant angular momentum coupling coefficients involving the first term vanish. The final result reads

$$B(E2; nLn_{\gamma}K \rightarrow n'L'n'_{\gamma}K') = \frac{5}{16\pi} t^2 (\langle L2L'|K, K' - K, K'\rangle)^2 B_{n,L,n',L'}^2 C_{n_{\gamma},K,n'_{\gamma},K'}^2, \quad (33)$$

where

$$B_{n,L,n',L'} = \int \beta F_n^L(\beta) F_{n'}^{L'}(\beta) \beta^4 d\beta \quad (34)$$

is the integral over  $\beta$ , while  $C_{n_{\gamma},K,n'_{\gamma},K'}$  is the integral over  $\gamma$ , in agreement to Ref. [8]. In ground  $\rightarrow$  ground,  $\beta \rightarrow$  ground,  $\beta \rightarrow \beta$  and  $\gamma \rightarrow \gamma$  transitions ( $\Delta K = 0$  transitions), the integral over  $\gamma$  becomes  $C_{n_{\gamma},K,n'_{\gamma},K'} = \delta_{n_{\gamma},n'_{\gamma}} \delta_{K,K'}$ , since (considering  $\cos \gamma \approx 1$ ) it corresponds to the relevant orthonormality condition of the  $\gamma$  wavefunctions, while in  $\gamma \rightarrow$  ground and  $\gamma \rightarrow \beta$  transitions ( $\Delta K = 2$  transitions) this integral has the form

$$C_{n_{\gamma},K,n'_{\gamma},K'} = \int \sin \gamma \eta_{n_{\gamma},|K|} \eta_{n'_{\gamma},|K'|} |\sin 3\gamma| d\gamma, \quad (35)$$

since the volume element is [1]

$$d\tau = \beta^4 |\sin 3\gamma| \sin \theta d\beta d\gamma d\theta d\phi d\psi. \quad (36)$$

For the bands considered here one needs the special cases of Eq. (22)

$$\eta_{0,0} = C_{0,0} e^{-(3c)\gamma^2/2}, \quad \eta_{1,2} = C_{1,2} \gamma e^{-(3c)\gamma^2/2}, \quad (37)$$

where the Laguerre polynomials are unity since  $\tilde{n} = 0$  in both cases, as seen from Eq. (22), the relevant normalization conditions being

$$(C_{0,0})^2 \int e^{-(3c)\gamma^2} |\sin 3\gamma| d\gamma = 1, \quad (C_{1,2})^2 \int \gamma^2 e^{-(3c)\gamma^2} |\sin 3\gamma| d\gamma = 1. \quad (38)$$

Then Eq. (35) takes the form

$$C_{1,2,0,0} = C_{0,0} C_{1,2} \int \gamma^2 e^{-(3c)\gamma^2} |\sin 3\gamma| d\gamma, \quad (39)$$

in which the integral is the same as the one appearing in the second normalization condition in Eq. (38), resulting in

$$C_{1,2,0,0} = \frac{C_{0,0}}{C_{1,2}}. \quad (40)$$

Using the approximation  $|\sin 3\gamma| \approx 3|\gamma|$  and the integral

$$\int_0^\infty x^m e^{-ax^2} dx = \frac{\Gamma\left(\frac{m+1}{2}\right)}{2a^{\frac{m+1}{2}}}$$

the normalization conditions give

$$(C_{0,0})^2 = 2c, \quad (C_{1,2})^2 = 6c^2, \quad \frac{C_{0,0}}{C_{1,2}} = \frac{1}{\sqrt{3c}}.$$

The normalization is consistent with the one used by Bohr [1]. The same approximations are also used in Ref. [44].

## Appendix III: ES-X(5)

In the case of the ES-X(5) solution [24], in which  $u(\beta)$  is an infinite well potential

$$u(\beta) = \begin{cases} 0 & \text{if } \beta \leq \beta_W \\ \infty & \text{for } \beta > \beta_W \end{cases}, \quad (41)$$

the  $\beta$ -equation becomes a Bessel equation with energy eigenvalues [3]

$$\epsilon_{\beta;s,L} = (k_{s,L})^2, \quad k_{s,L} = \frac{x_{s,L}}{\beta_W}, \quad (42)$$

where  $x_{s,L}$  is the  $s$ -th zero of the Bessel function  $J_\nu(k_{s,L}\beta)$  with

$$\nu = \sqrt{\frac{L(L+1) - K^2}{3} + \frac{9}{4} + 3C(n_\gamma + 1)}, \quad (43)$$

while the relevant eigenfunctions are

$$\xi_{s,L}(\beta) = C_{s,L} \beta^{-3/2} J_\nu(k_{s,L}\beta), \quad (44)$$

where  $C_{s,L}$  are normalization constants, determined from the condition

$$\int_0^{\beta_W} \beta^4 \xi_{s,L}^2(\beta) d\beta = 1, \quad (45)$$

leading to

$$\frac{1}{C_{s,L}^2} = \frac{\beta_W^2}{2} J_{\nu+1}^2(x_{s,L}). \quad (46)$$

The full wave function reads

$$\Psi(\beta, \gamma, \theta_i) = C_{s,L} \beta^{-3/2} J_\nu(k_{s,L} \beta) \eta_{n_\gamma, |K|}(\gamma) \mathcal{D}_{MK}^L(\theta_i), \quad (47)$$

and should be properly symmetrized [43]

$$\Psi(\beta, \gamma, \theta_i) = C_{s,L} \beta^{-3/2} J_\nu(k_{s,L} \beta) \eta_{n_\gamma, |K|}(\gamma) \sqrt{\frac{2L+1}{16\pi^2(1+\delta_{K,0})}} \left( \mathcal{D}_{M,K}^L + (-1)^L \mathcal{D}_{M,-K}^L \right). \quad (48)$$

In calculating  $B(E2)$ s, the integrals over  $\gamma$  and the Euler angles remain the same as in Appendix II, while the integrals over  $\beta$  take the form

$$B_{s,L,s',L'} = C_{s,L} C_{s',L'} \int \beta J_\nu(k_{s,L} \beta) J_{\nu'}(k_{s',L'} \beta) \beta d\beta, \quad (49)$$

where the formal correspondence  $n = s - 1$  holds.

It should be noticed at this point that for  $C = 0$  the numerical results of ES-X(5) for the ground state band and the beta bands coincide with the results of X(5), as it can be seen from Eq. (43). As discussed at the end of Appendix I, this should be considered as a numerical coincidence, because  $C = 0$  is not allowed in the X(5) framework, since it destroys the  $\gamma \approx 0$  approximation.

## References

- [1] A. Bohr, Mat. Fys. Medd. K. Dan. Vidensk. Selsk. **26**, no. 14 (1952).
- [2] F. Iachello, Phys. Rev. Lett. **85**, 3580 (2000).
- [3] F. Iachello, Phys. Rev. Lett. **87**, 052502 (2001).
- [4] L. Wilets and M. Jean, Phys. Rev. **102**, 788 (1956).
- [5] J. Meng, W. Zhang, S.G. Zhou, H. Toki and L.S. Geng, Eur. Phys. J. **25**, 23 (2005).
- [6] Z.-Q. Sheng and J.-Y. Guo, Mod. Phys. Lett. A **20**, 2711 (2005).
- [7] R. Fossion, D. Bonatsos and G.A. Lalazissis, Phys. Rev. C **73**, 044310 (2006).
- [8] R. Bijker, R.F. Casten, N.V. Zamfir and E.A. McCutchan, Phys. Rev. C **68**, 064304 (2003).
- [9] S.M. Harris, Phys. Rev. Lett. **13**, 663 (1964).
- [10] M.A.J. Mariscotti, G. Sharf-Goldhaber and B. Buck, Phys. Rev. **178**, 1864 (1969).
- [11] H. Ejiri, M. Ishihara, M. Sakai, K. Katori and T. Inamura, J. Phys. Soc. Jpn. **24**, 1189 (1968).
- [12] P. Holmberg and P.O. Lipas, Nucl. Phys. A **117**, 552 (1968).

- [13] R.F. Casten and N.V. Zamfir, Phys. Rev. Lett. **87**, 052503 (2001).
- [14] R. Krücken *et al.*, Phys. Rev. Lett. **88**, 232501 (2002).
- [15] N. Pietralla and O. M. Gorbachenko, Phys. Rev. C **70**, 011304 (R) (2004).
- [16] K. Dusling and N. Pietralla, Phys. Rev. C **72**, 011303(R) (2005).
- [17] L. Fortunato, Eur. Phys. J. A **26**, s01, 1 (2005).
- [18] L. Fortunato, Phys. Rev. C **70**, 011302 (2004).
- [19] L. Fortunato, S. De Baerdemacker and K. Heyde, Phys. Rev. C **74**, 014310 (2006).
- [20] M.A. Caprio, Phys. Rev. C **72**, 054323 (2005).
- [21] D. J. Rowe, Nucl. Phys. A **735**, 372 (2004).
- [22] D. J. Rowe, P. S. Turner and J. Repka, J. Math. Phys. **45**, 2761 (2004).
- [23] D. J. Rowe and P. S. Turner, Nucl. Phys. A **753**, 94 (2005).
- [24] D. Bonatsos, D. Lenis, E.A. McCutchan, D. Petrellis and I. Yigitoglu, Phys. Lett. B **649**, 394 (2007).
- [25] P.M. Davidson, Proc. R. Soc. London, Ser. A **135**, 459 (1932).
- [26] D. Bonatsos, D. Lenis, N. Minkov, D. Petrellis, P.P. Raychev and P.A. Terziev, Phys. Lett. B **584**, 40 (2004).
- [27] D. Bonatsos, D. Lenis, N. Minkov, D. Petrellis, P.P. Raychev and P.A. Terziev, Phys. Rev. C **70**, 024305 (2004).
- [28] J. P. Elliott, J. A. Evans and P. Park, Phys. Lett. B **169**, 309 (1986).
- [29] F. Iachello and A. Arima, *The Interacting Boson Model* (Cambridge University Press, Cambridge, 1987).
- [30] J. P. Elliott, P. Park, and J. A. Evans, Phys. Lett. B **171**, 145 (1986).
- [31] D. J. Rowe and C. Bahri, J. Phys. A **31**, 4947 (1998).
- [32] D. J. Rowe and G. Thiamova, Nucl. Phys. A **760**, 59 (2005).
- [33] G. Thiamova and D. J. Rowe, Czech. J. Phys. **55**, 957 (2005).
- [34] D. J. Rowe, J. Phys. A **38**, 10181 (2005).
- [35] Ch. Hinke, R. Krücken, R. F. Casten, V. Werner and N. V. Zamfir, Eur. Phys. J. A **30**, 357 (2006).
- [36] F. Iachello, in *Symmetries and Low-Energy Phase Transition in Nuclear-Structure Physics*, edited by G. Lo Bianco (U. Camerino, Camerino, 2006) p. 1.

- [37] A. C. Gheorghe, A. A. Raduta, and A. Faessler, Phys. Lett. B **648**, 171 (2007).
- [38] M. Jean, Nucl. Phys. **21**, 142 (1960).
- [39] F. Cooper, A. Khare, and U. Sukhatme, *Supersymmetry in Quantum Mechanics* (World Scientific, Singapore, 2001).
- [40] S. De Baerdemacker, L. Fortunato, V. Hellemans, and K. Heyde, Nucl. Phys. A **769**, 16 (2006).
- [41] M.A. Caprio, Phys. Rev. C **69**, 044307 (2004).
- [42] M. Moshinsky, J. Math. Phys. **25**, 1555 (1984).
- [43] J. M. Eisenberg and W. Greiner, *Nuclear Theory, Vol. 1: Nuclear Models* (North Holland, Amsterdam, 1975).
- [44] J. P. Davidson, *Collective Models of the Nucleus* (Academic, New York, 1968).
- [45] Nuclear Data Sheets, as of December 2005.
- [46] N. V. Zamfir, P. von Brentano, R. F. Casten and J. Jolie, Phys. Rev. C **66**, 021304 (2002).
- [47] V. Werner, P. von Brentano, R. F. Casten and J. Jolie, Phys. Lett. B **527**, 55 (2002).
- [48] J. Jolie, R. F. Casten, P. Cejnar, S. Heinze, E. A. McCutchan and N. V. Zamfir, Phys. Rev. Lett. **93**, 132501 (2004).
- [49] Y. Alhassid and N. Whelan, Phys. Rev. Lett. **67**, 816 (1991).
- [50] R. F. Casten, *Nuclear Structure from a Simple Perspective* (Oxford University Press, Oxford, 1990).
- [51] D. Bonatsos, D. Lenis, N. Minkov, P. P. Raychev, and P. A. Terziev, Phys. Rev. C **69**, 014302 (2004).

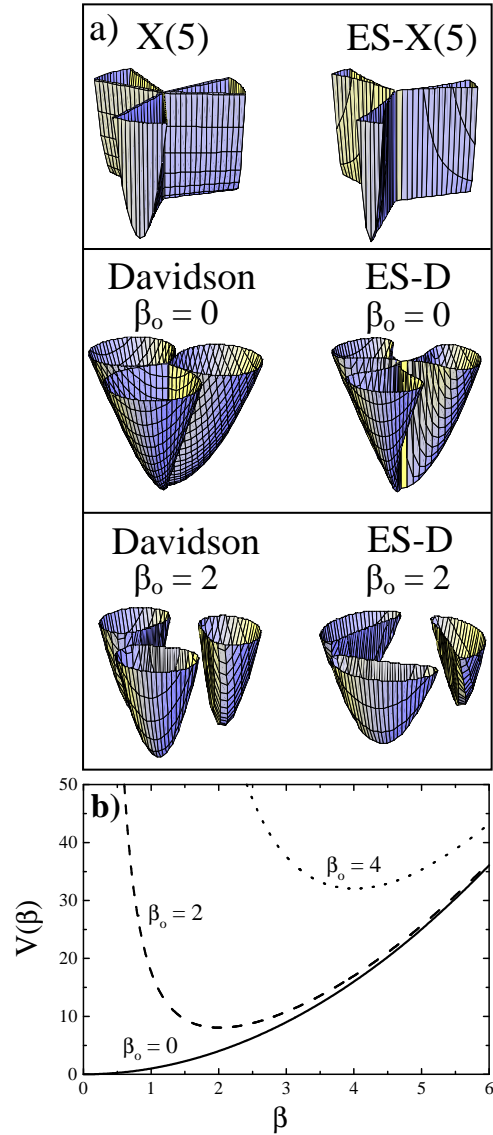


Figure 1: (a) Potentials in both the  $\beta$  and  $\gamma$  degrees of freedom for X(5) (top) and the Davidson potential with  $\beta_0 = 0$  (middle) and  $\beta_0 = 2$  (bottom). Potentials are shown for the approximate separation of variables (left) and the exact separation of the variables (right). (b) Davidson potential in the  $\beta$  degree of freedom for a few values of the parameter  $\beta_0$ .

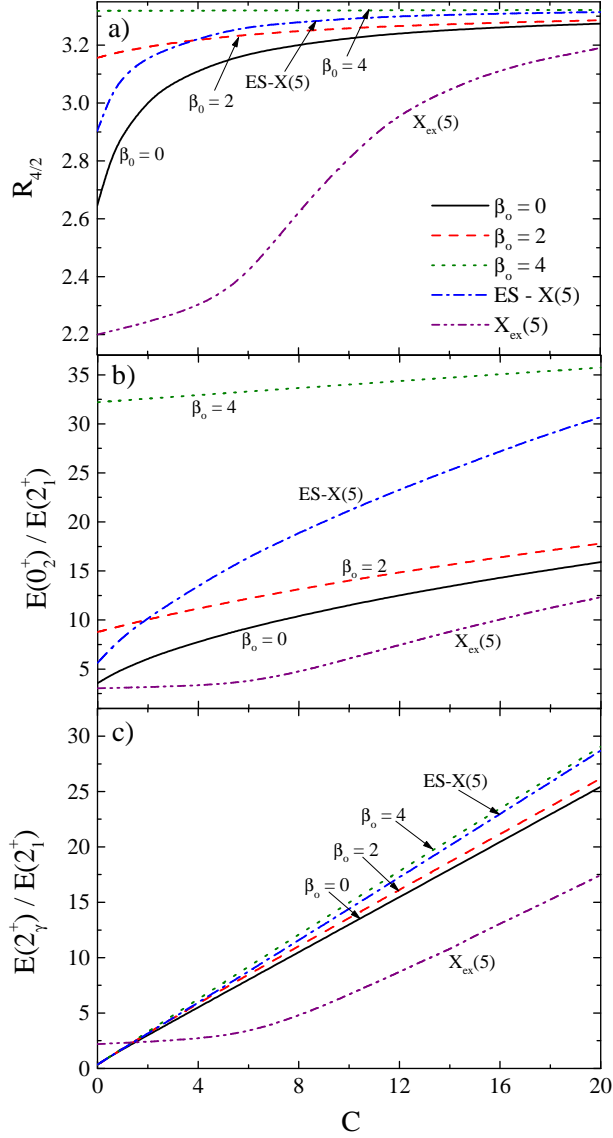


Figure 2: (Color online) (a) The  $R_{4/2} = E(4_1^+)/E(2_1^+)$  ratio as a function of the parameter  $C$  for the ES-D solution (for different values of the Davidson parameter  $\beta_0$ ), the ES-X(5) solution, and for the  $X_{\text{ex}}(5)$  solution [20]. The  $X_{\text{ex}}(5)$  parameter  $a$  is connected to parameter  $C$  of the present solution through the relation  $C = (2/3)\sqrt{a}$ . (b) Same as (a), but for the ratio  $R_{0/2} = E(0_2^+)/E(2_1^+)$ , corresponding to the normalized  $\beta$  bandhead energy. (c) Same as (a), but for the ratio  $R_{2/2} = E(2_\gamma^+)/E(2_1^+)$ , corresponding to the normalized  $\gamma$  bandhead energy. See subsec. 3.1 for further discussion.

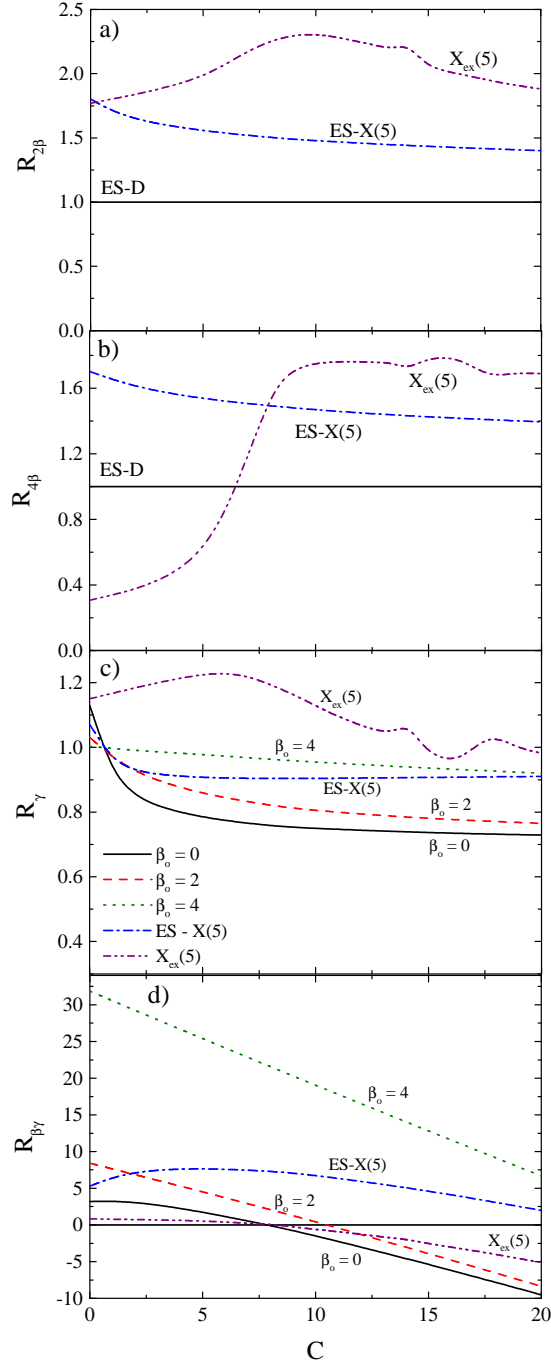


Figure 3: (Color online) Energy ratios (a)  $R_{2\beta} = \frac{E(2_{\beta}^+) - E(0_{\beta}^+)}{E(2_1^+)}$  [Eq. (8)], (b)  $R_{4\beta} = \frac{E(4_{\beta}^+) - E(2_{\beta}^+)}{E(4_1^+) - E(2_1^+)}$  [Eq. (9)], (c)  $R_{\gamma} = \frac{E(4_1^+) - E(2_1^+)}{E(4_1^+) - E(2_1^+)}$  [Eq. (10)], and (d)  $R_{\beta\gamma} = \frac{E(0_{\beta}^+) - E(2_{\gamma}^+)}{E(2_1^+)}$  [Eq. (11)] as functions of the parameter  $C$ , for the same solutions shown in Fig. 2. See subsec. 3.2 for further discussion.

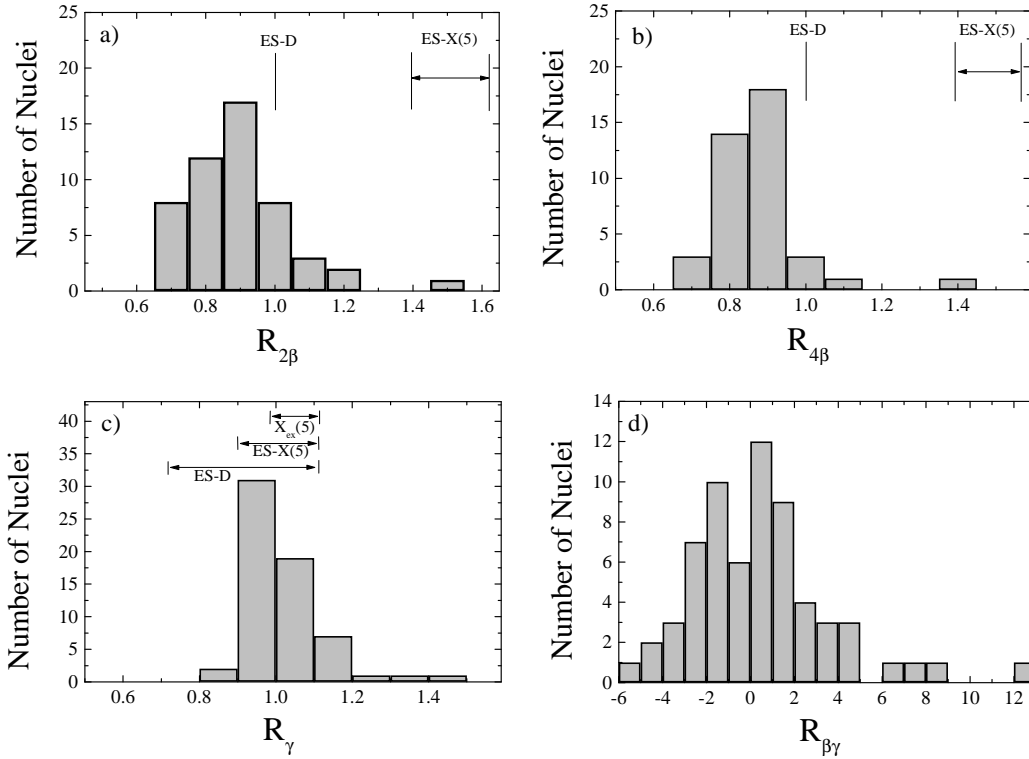


Figure 4: Experimental data for the same energy ratios shown in Fig. 3. For each ratio, all nuclei with  $A > 100$  and  $R_{4/2} > 3.0$  for which sufficient experimental data (taken from Ref. [45]) exist, have been taken into account. The predictions for ES-D, ES-X(5) and  $X_{ex}(5)$  are indicated in (a), (b), and (c). The  $X_{ex}(5)$  predictions lie off scale to the right in (a) and (b). See subsec. 3.2 for further discussion.

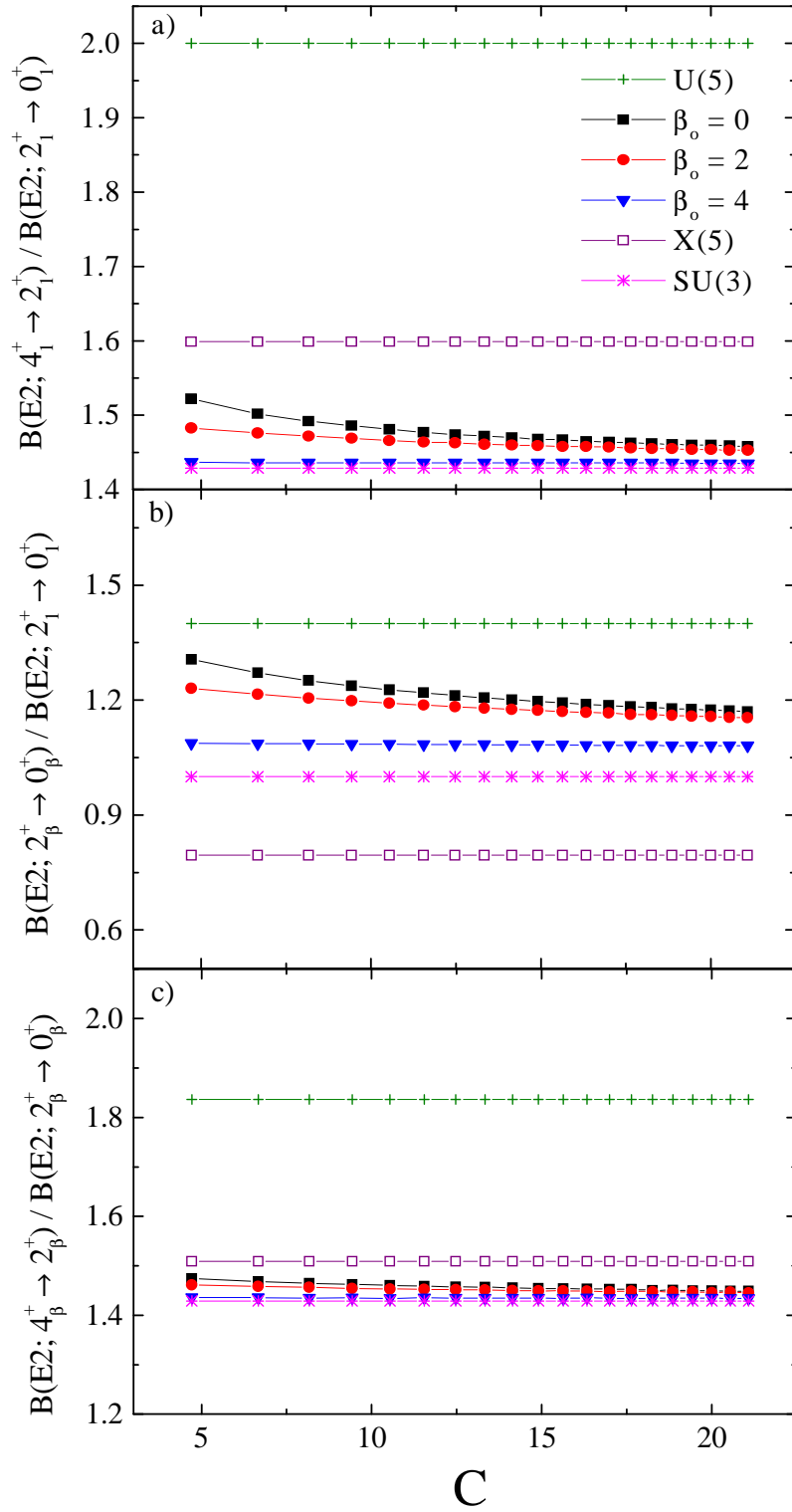


Figure 5: (Color online) Intraband  $B(E2)$  ratios for the ground state and  $\beta$  bands vs. the parameter  $C$  as predicted by the ES-D model (labelled by the value of the  $\beta_0$  parameter), compared to U(5) [29], X(5) [3, 8], and SU(3) [29] predictions, as described in subsec. 3.3.

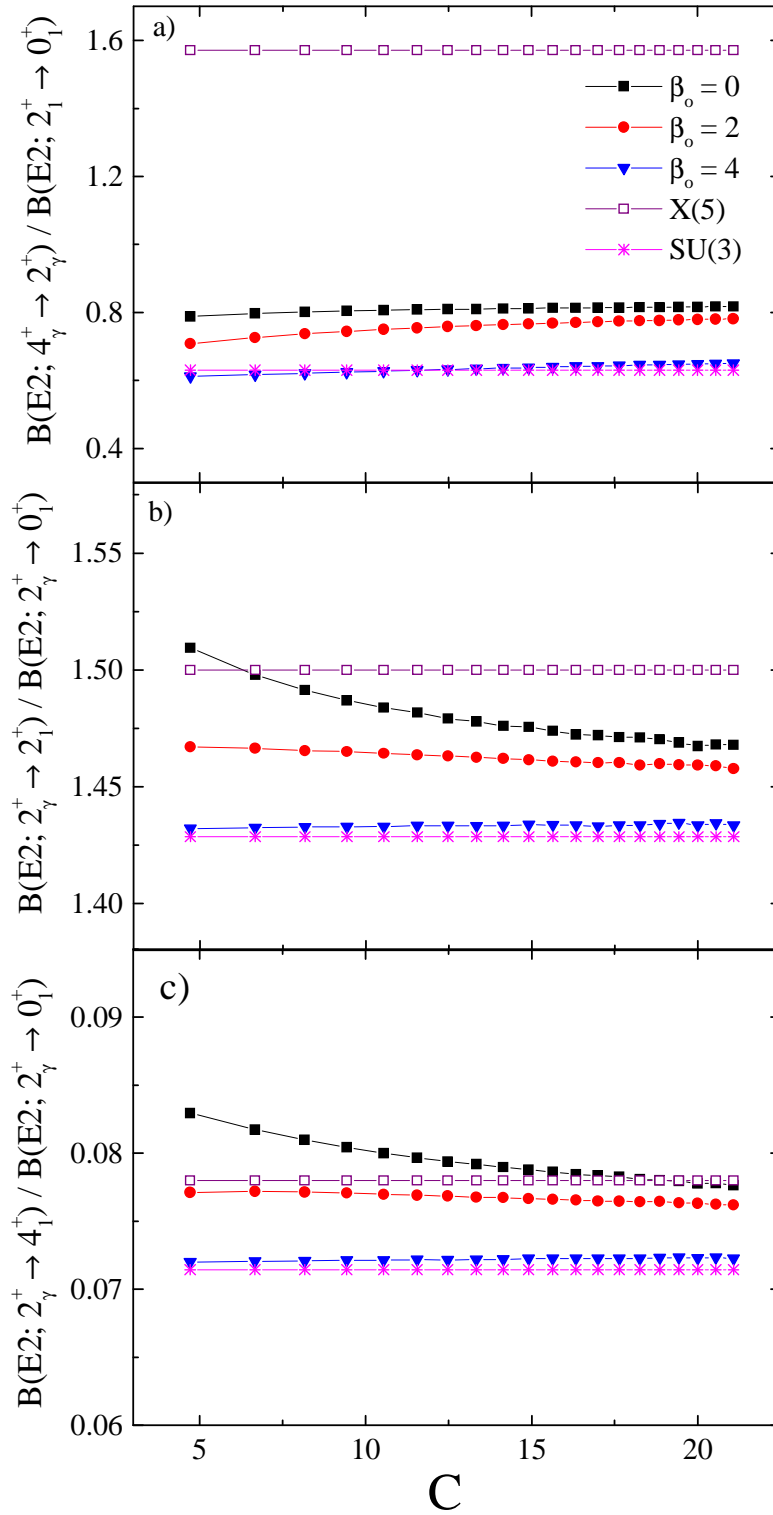


Figure 6: (Color online)  $B(E2)$  ratios from the  $\gamma$  band vs. the parameter  $C$  as predicted by the ES-D model (labelled by the value of the  $\beta_0$  parameter), compared to the X(5) [3, 8] and SU(3) [29] predictions, as described in subsec. 3.3.

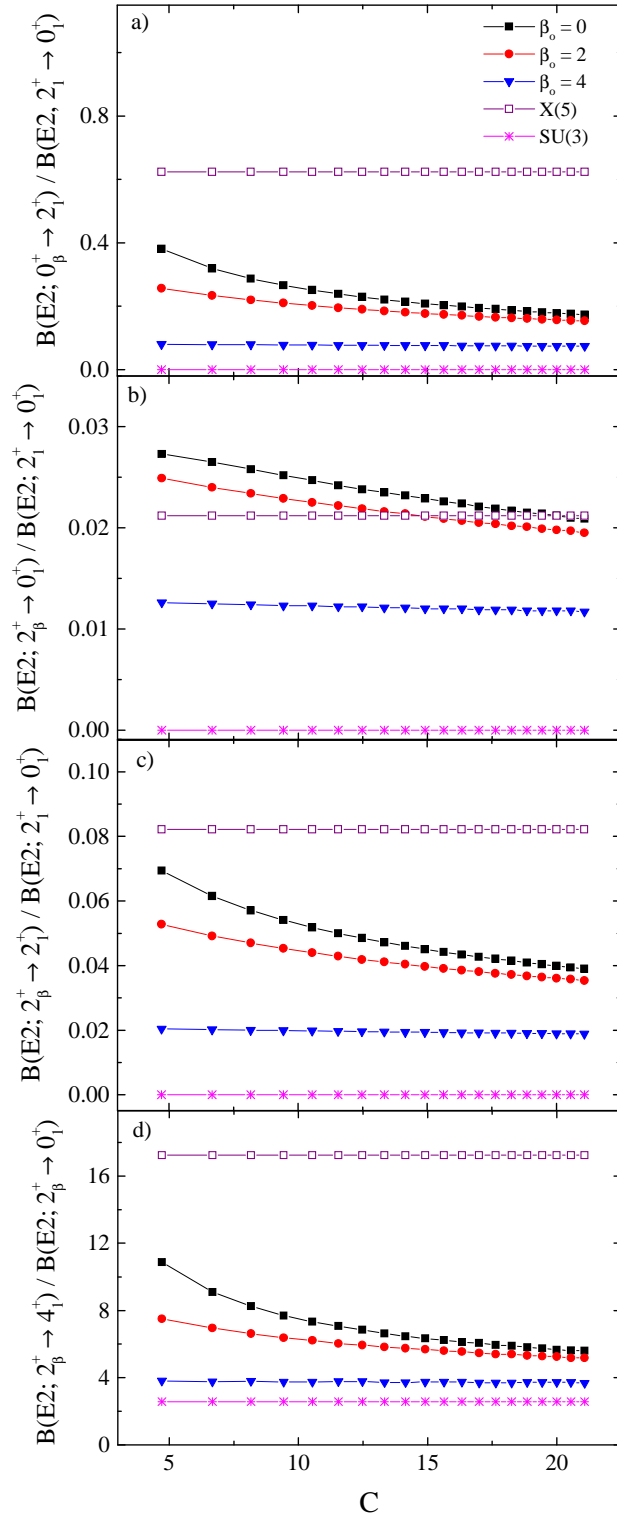


Figure 7: (Color online)  $B(E2)$  ratios from the  $\beta$  band vs. the parameter  $C$  as predicted by the ES-D model (labelled by the value of the  $\beta_0$  parameter), compared to the X(5) [3, 8] and SU(3) [29] predictions, as described in subsec. 3.3.

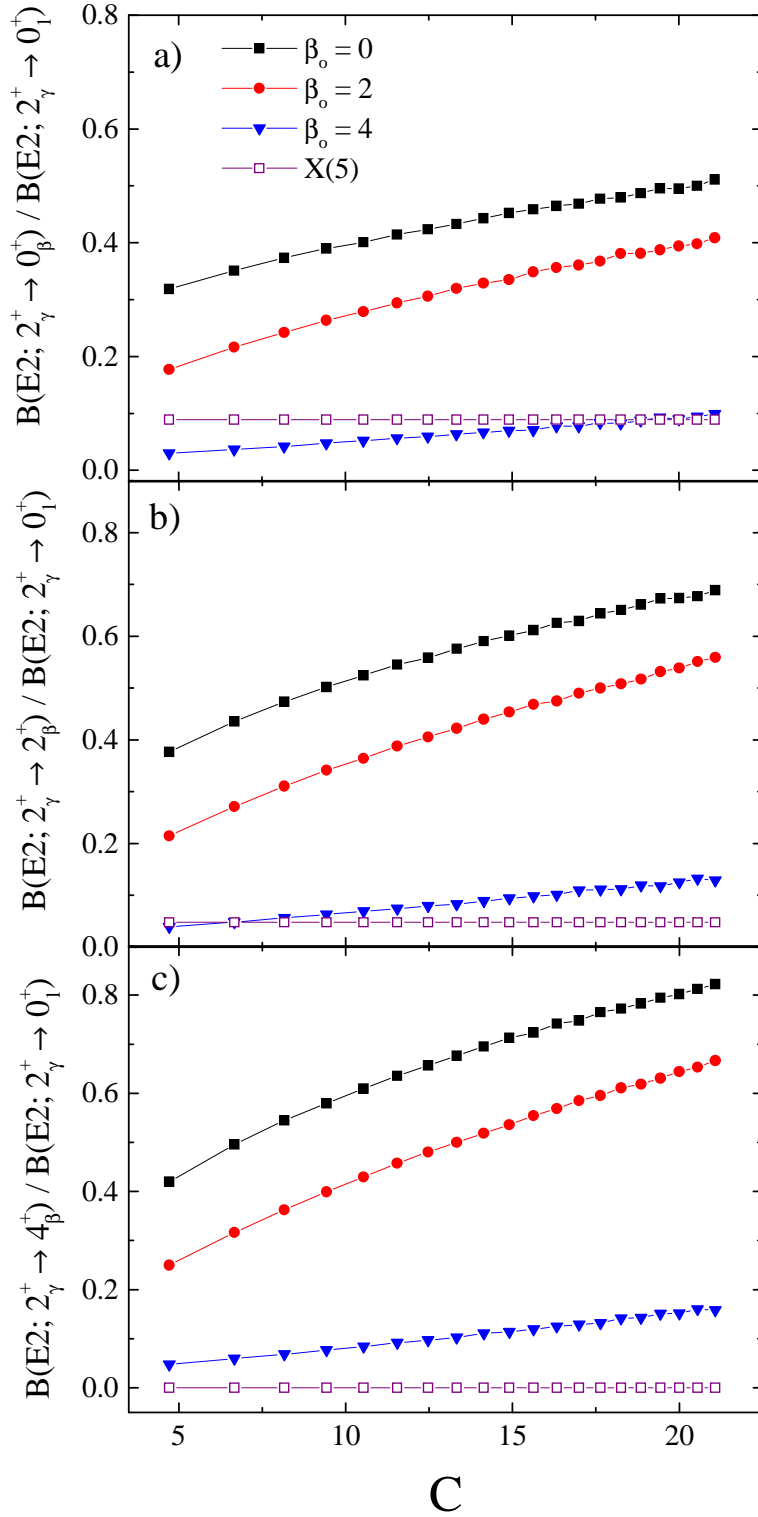


Figure 8: (Color online)  $B(E2)$  ratios between the  $\gamma$  band and  $\beta$  band vs. the parameter  $C$  as predicted by the ES-D model (labelled by the value of the  $\beta_0$  parameter), compared to the X(5) [3, 8] predictions, as described in subsec. 3.3.

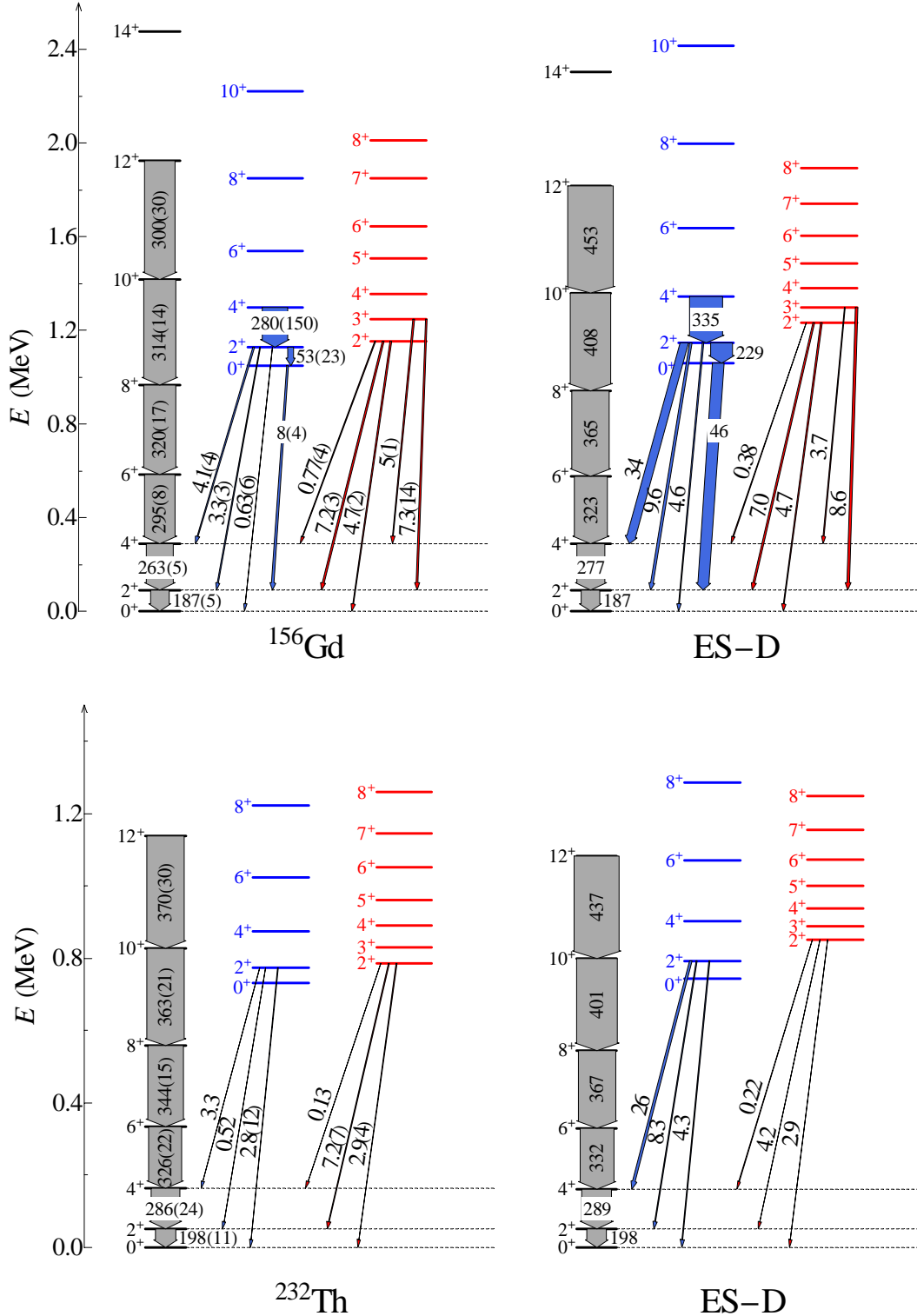


Figure 9: (Color online) Experimental [45] level schemes (left) compared to ES-D predictions (right) for  $^{156}\text{Gd}$  (top) and  $^{232}\text{Th}$  (bottom) using the parameter sets given in Table 1.  $\Delta K = 0$  transitions are normalized to  $2_1^+ \rightarrow 0_1^+$ , while  $\Delta K = 2$  transitions are normalized to  $2_\gamma^+ \rightarrow 0_1^+$ .

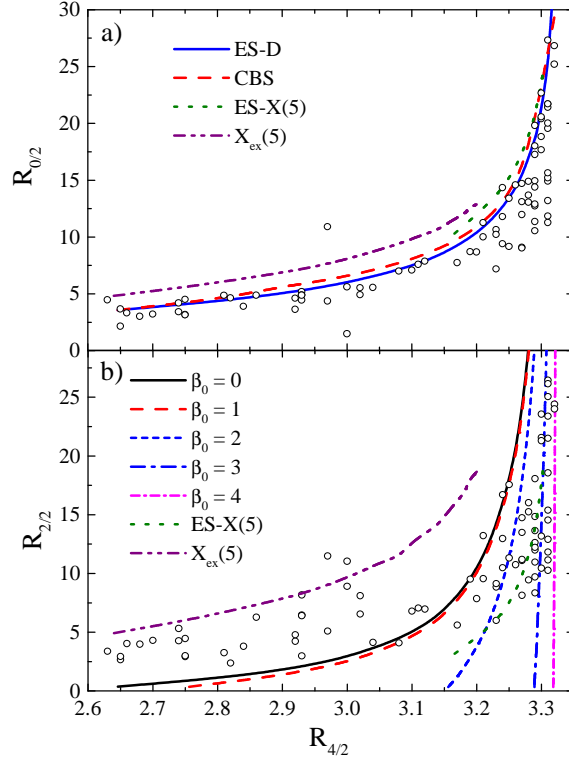


Figure 10: (Color online) (a) Experimental data [45] for the normalized  $\beta$  bandhead energies  $R_{0/2} = E(0_{\beta}^+)/E(2_1^+)$  vs. the energy ratio  $R_{4/2} = E(4_1^+)/E(2_1^+)$ , compared to predictions of the the ES-D and ES-X(5) solutions, as well as to the predictions of the confined  $\beta$ -soft (CBS) solution [15, 16]. (b) Same as (a), but for the normalized  $\gamma$  bandheads  $R_{2/2} = E(2_{\gamma}^+)/E(2_1^+)$ . See subsection 3.5 for further discussion.

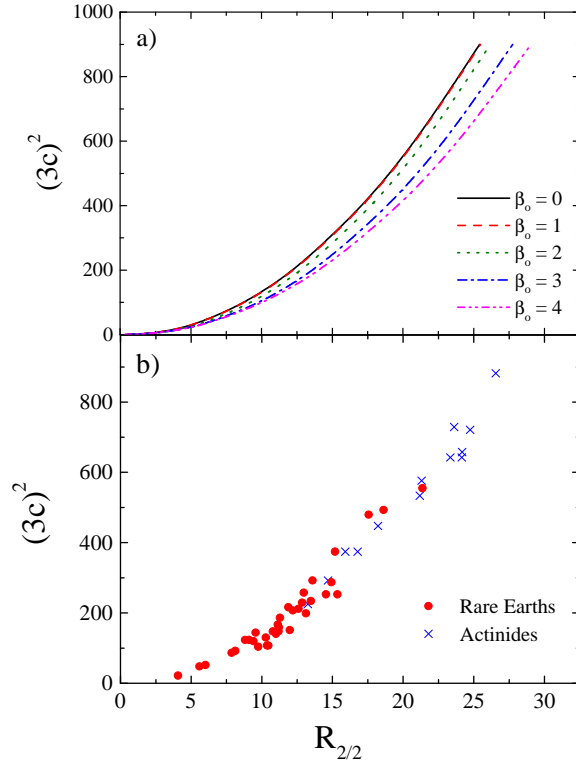


Figure 11: (Color online) (a) The gamma-stiffness coefficient  $(3c)^2$  is shown as a function of the normalized  $\gamma$  bandhead energy  $R_{2/2} = E(2_\gamma^+)/E(2_1^+)$  predicted by the ES-D solution for different values of the Davidson parameter  $\beta_0$ . (b) Same as (a), but for the rare earth and actinide nuclei appearing in Table 1 . See subsec. 3.6 for further discussion.

Table 1: Comparison of theoretical predictions of the exactly separable Davidson solution [ES-D] to experimental data[45] of rare earth and actinides with  $R_{4/2} > 3.0$  and known  $0_2^+$  and  $2_\gamma^+$  states. The  $R_{4/2} = E(4_1^+)/E(2_1^+)$  ratios, as well as the  $\beta$  and  $\gamma$  bandheads, normalized to the  $2_1^+$  state and labelled by  $R_{0/2} = E(0_\beta^+)/E(2_1^+)$  and  $R_{2/2} = E(2_\gamma^+)/E(2_1^+)$  respectively, are shown. The angular momenta of the highest levels of the ground state,  $\beta$  and  $\gamma$  bands included in the rms fit are labelled by  $L_g$ ,  $L_\beta$ , and  $L_\gamma$  respectively, while  $n$  indicates the total number of levels involved in the fit and  $\sigma$  is the quality measure of Eq. (12). See subsec. 3.4 for further discussion.

nucleus	$R_{4/2}$ exp	$R_{4/2}$ th	$R_{0/2}$ exp	$R_{0/2}$ th	$R_{2/2}$ exp	$R_{2/2}$ th	$\beta_0$	$C$	$L_g$	$L_\beta$	$L_\gamma$	$n$	$\sigma$
<sup>154</sup> Sm	3.25	3.26	13.4	14.1	17.6	18.8	1.26	14.6	16	6	7	17	1.025
<sup>156</sup> Gd	3.24	3.23	11.8	11.9	13.0	13.9	0.0	10.7	14	10	8	19	1.044
<sup>158</sup> Gd	3.29	3.27	15.0	14.8	14.9	15.3	2.05	11.3	12	6	6	14	0.624
<sup>160</sup> Gd	3.30	3.29	17.6	18.3	13.1	13.4	2.69	9.4	16	4	8	17	0.962
<sup>162</sup> Gd	3.29	3.30	19.8	20.2	12.0	12.0	2.93	8.2	14	0	4	10	0.335
<sup>158</sup> Dy	3.21	3.20	10.0	10.4	9.6	10.5	0.0	8.0	14	8	8	18	0.928
<sup>160</sup> Dy	3.27	3.27	14.7	15.8	11.1	12.1	2.40	8.6	28	4	23	38	0.633
<sup>162</sup> Dy	3.29	3.29	17.3	17.7	11.0	11.4	2.68	7.9	18	6	11	22	1.109
<sup>164</sup> Dy	3.30	3.30	22.6	22.5	10.4	10.3	3.18	6.9	20	0	10	19	0.089
<sup>166</sup> Dy	3.31	3.27	15.0	14.9	11.2	11.4	2.30	8.1	6	2	5	8	0.166
<sup>160</sup> Er	3.10	3.15	7.1	8.7	6.8	7.0	0.0	5.2	14	2	5	12	0.815
<sup>162</sup> Er	3.23	3.23	10.7	11.6	8.8	10.1	1.68	7.4	12	4	11	18	0.942
<sup>164</sup> Er	3.28	3.26	13.6	13.9	9.4	10.3	2.19	7.3	14	6	11	20	0.937
<sup>166</sup> Er	3.29	3.28	18.1	17.3	9.8	9.9	2.68	6.8	16	8	13	24	0.397
<sup>168</sup> Er	3.31	3.27	15.3	15.0	10.3	10.8	2.34	7.6	12	6	8	16	0.892
<sup>170</sup> Er	3.31	3.23	11.3	11.7	11.9	12.8	1.09	9.8	10	4	7	13	0.978
<sup>164</sup> Yb	3.13	3.20	7.9	10.1	7.0	7.5	1.58	5.4	18	0	5	13	0.807
<sup>166</sup> Yb	3.23	3.20	10.2	10.5	9.1	9.8	1.18	7.4	12	6	7	15	0.774
<sup>168</sup> Yb	3.27	3.25	13.2	13.5	11.2	11.6	2.03	8.4	14	4	7	15	0.532
<sup>170</sup> Yb	3.29	3.25	12.7	13.2	13.6	15.0	1.56	11.4	12	6	11	19	1.168
<sup>172</sup> Yb	3.31	3.26	13.2	13.8	18.6	19.0	0.0	14.8	12	8	5	14	1.078
<sup>174</sup> Yb	3.31	3.30	19.4	20.0	21.4	21.7	2.66	15.7	16	4	5	14	0.956
<sup>176</sup> Yb	3.31	3.30	21.7	22.4	15.4	15.4	3.08	10.6	18	0	2	10	0.386
<sup>178</sup> Yb	3.31	3.27	15.7	15.5	14.5	14.6	2.24	10.6	6	4	2	6	0.128
<sup>168</sup> Hf	3.11	3.16	7.6	9.0	7.1	7.5	0.0	5.6	14	2	4	11	0.814
<sup>170</sup> Hf	3.19	3.20	8.7	10.2	9.5	10.0	0.0	7.6	14	2	4	11	0.835
<sup>172</sup> Hf	3.25	3.22	9.2	11.1	11.3	11.9	0.0	9.1	12	2	6	12	1.142
<sup>174</sup> Hf	3.27	3.23	9.1	11.6	13.5	13.2	0.0	10.2	10	2	4	9	1.471
<sup>176</sup> Hf	3.28	3.25	13.0	13.1	15.2	16.6	0.99	12.9	12	6	8	16	1.040
<sup>178</sup> Hf	3.29	3.25	12.9	13.3	12.6	13.1	1.86	9.7	14	6	6	15	1.099
<sup>180</sup> Hf	3.31	3.23	11.8	12.0	12.9	13.2	1.26	10.1	10	4	5	11	0.830

Table 1: (continued)

nucleus	$R_{4/2}$ exp	$R_{4/2}$ th	$R_{0/2}$ exp	$R_{0/2}$ th	$R_{2/2}$ exp	$R_{2/2}$ th	$\beta_0$	$C$	$L_g$	$L_\beta$	$L_\gamma$	$n$	$\sigma$
$^{176}\text{W}$	3.22	3.20	7.8	10.1	9.6	9.9	0.0	7.5	12	2	5	11	1.281
$^{178}\text{W}$	3.24	3.19	9.4	9.8	10.5	9.1	0.0	6.9	12	8	2	11	1.260
$^{180}\text{W}$	3.26	3.27	14.6	14.7	10.8	11.4	2.27	8.1	12	0	7	12	0.313
$^{182}\text{W}$	3.29	3.24	11.3	12.4	12.2	12.8	1.60	9.6	12	4	6	13	1.136
$^{184}\text{W}$	3.27	3.18	9.0	9.7	8.1	8.6	0.98	6.4	10	4	6	12	0.928
$^{186}\text{W}$	3.23	3.14	7.2	8.4	6.0	6.5	0.0	4.8	10	4	6	12	1.142
$^{180}\text{Os}$	3.09	3.15	5.6	8.6	6.6	6.9	0.0	5.1	14	6	7	16	1.348
$^{184}\text{Os}$	3.20	3.21	8.7	10.6	7.9	8.5	1.58	6.2	12	0	6	11	0.918
$^{186}\text{Os}$	3.17	3.14	7.7	8.3	5.6	6.3	0.0	4.6	10	10	9	18	0.982
$^{188}\text{Os}$	3.08	3.13	7.0	8.1	4.1	4.5	1.42	3.1	12	2	7	13	0.571
$^{228}\text{Ra}$	3.21	3.23	11.3	11.5	13.3	13.0	0.0	10.0	6	4	3	7	0.447
$^{228}\text{Th}$	3.24	3.26	14.4	14.5	16.8	17.1	1.79	12.9	18	2	5	14	0.240
$^{230}\text{Th}$	3.27	3.24	11.9	12.3	14.7	14.7	0.0	11.4	12	4	4	11	0.864
$^{232}\text{Th}$	3.28	3.27	14.8	15.0	15.9	17.2	1.95	12.9	14	20	12	28	1.030
$^{232}\text{U}$	3.29	3.26	14.5	14.6	18.2	18.5	1.67	14.1	14	10	4	15	0.910
$^{234}\text{U}$	3.30	3.29	18.6	19.0	21.3	21.8	2.50	16.0	18	8	7	19	0.634
$^{236}\text{U}$	3.30	3.30	20.3	20.8	21.2	21.4	2.77	15.4	18	4	5	15	0.686
$^{238}\text{U}$	3.30	3.30	20.6	21.7	23.6	24.8	2.79	18.0	18	4	15	25	0.845
$^{238}\text{Pu}$	3.31	3.30	21.4	22.0	23.3	23.5	2.86	16.9	16	2	4	12	0.839
$^{240}\text{Pu}$	3.31	3.30	20.1	20.5	26.6	26.8	2.56	19.8	16	4	4	13	0.878
$^{242}\text{Pu}$	3.31	3.30	21.5	21.9	24.7	24.7	2.82	17.9	16	2	2	10	0.740
$^{248}\text{Cm}$	3.31	3.31	25.0	25.4	24.2	24.2	3.21	17.1	20	4	2	13	0.520
$^{250}\text{Cf}$	3.32	3.31	27.0	26.9	24.2	24.1	3.36	16.9	8	2	4	8	0.067

Table 2: Comparison of several  $B(E2)$  ratios predicted (lower line) by the exactly separable Davidson solution [ES-D], for the parameter values shown in Table 1, to experimental data[45] (upper line) of several nuclei where the relevant data are known. See subsec. 3.4 for further discussion.

nucleus	$\frac{4_1 \rightarrow 2_1}{2_1 \rightarrow 0_1}$	$\frac{6_1 \rightarrow 4_1}{2_1 \rightarrow 0_1}$	$\frac{8_1 \rightarrow 6_1}{2_1 \rightarrow 0_1}$	$\frac{10_1 \rightarrow 8_1}{2_1 \rightarrow 0_1}$	$\frac{2_\beta \rightarrow 0_1}{2_1 \rightarrow 0_1}$ x $10^3$	$\frac{2_\beta \rightarrow 2_1}{2_1 \rightarrow 0_1}$ x $10^3$	$\frac{2_\beta \rightarrow 4_1}{2_1 \rightarrow 0_1}$ x $10^3$	$\frac{2_\gamma \rightarrow 2_1}{2_\gamma \rightarrow 0_1}$	$\frac{2_\gamma \rightarrow 4_1}{2_\gamma \rightarrow 0_1}$
$^{154}\text{Sm}$	1.40(5) 1.47	1.67(7) 1.69	1.83(11) 1.88	1.81(11) 2.06	5.4(13) 22.7		25(6) 44.5		0.21(5) 0.08
$^{156}\text{Gd}$	1.41(5) 1.48	1.58(6) 1.73	1.71(10) 1.95	1.68(9) 2.18	3.4(3) 24.6	18(2) 52	22(2) 179	1.55(7) 1.48	0.16(1) 0.08
$^{158}\text{Gd}$	1.46(5) 1.46		1.67(16) 1.86	1.72(16) 2.03	1.6(2) 22.1	0.4(1) 42.5	7.0(8) 133	1.77(26) 1.46	0.079(14) 0.077
$^{158}\text{Dy}$	1.45(10) 1.49	1.86(12) 1.77	1.86(38) 2.02	1.75(28) 2.29	12(3) 26	19(4) 58	66(16) 215	3.22(94) 1.49	0.36(15) 0.08
$^{160}\text{Dy}$	1.46(7) 1.46	1.23(7) 1.67	1.70(16) 1.84	1.69(9) 2.00	3.4(4) 21.3		8.5(10) 122	1.89(18) 1.45	0.13(1) 0.08
$^{162}\text{Dy}$	1.45(7) 1.45	1.51(10) 1.65	1.74(10) 1.80	1.76(13) 1.94		19.8 36.2		1.67(20) 1.45	0.14(1) 0.07
$^{164}\text{Dy}$	1.30(7) 1.45	1.56(7) 1.62	1.48(9) 1.75	1.69(9) 1.86		16.9 29.2		2.00(30) 1.44	0.24(3) 0.07
$^{162}\text{Er}$					8(7)		170(90)	2.37(25)	0.29(21)
	1.48	1.74	1.97	2.20	24.9	52.8	190	1.48	0.08
$^{164}\text{Er}$	1.18(13) 1.47		1.57(9) 1.88	1.64(11) 2.07		22.9 45.0		2.19(35) 1.46	0.33(5) 0.08
$^{166}\text{Er}$	1.45(12) 1.46	1.62(22) 1.65	1.71(25) 1.81	1.73(23) 1.95	20.1 36.9		107	1.76(18) 1.45	0.12(1) 0.07
$^{168}\text{Er}$	1.54(7) 1.46	2.13(16) 1.68	1.69(11) 1.85	1.46(11) 2.03		21.9 42.1		1.77(10) 1.46	0.129(9) 0.076
$^{170}\text{Er}$			1.78(15) 1.54(11)		1.4(1)	0.2(2)	6.8(12)		0.079(19)
	1.48	1.73	1.96	2.20	24.8	52.3	184	1.48	0.080
$^{166}\text{Yb}$	1.43(9) 1.49	1.53(10) 1.77	1.70(18) 2.02	1.61(80) 2.29		25.8 57.4		215 1.49	0.081
$^{168}\text{Yb}$					8.6(9)			2.09(50)	0.39(10)
	1.47	1.70	1.89	2.09	23.2	46.2	151	1.47	0.08
$^{170}\text{Yb}$			1.79(16) 1.77(14)		5.4(10)			1.78(50)	0.18(5)
	1.47	1.70	1.90	2.11	23.5	47.1	156	1.47	0.08
$^{172}\text{Yb}$	1.42(10) 1.47	1.51(14) 1.69	1.89(19) 1.88	1.77(11) 2.08	1.1(1) 22.9	3.7(6) 45.2	12(1) 146		0.097(11) 1.48
$^{174}\text{Yb}$	1.39(7) 1.45	1.84(26) 1.64	1.93(12) 1.77	1.67(12) 1.89		18.3 32.4		89 1.45	0.075
$^{176}\text{Yb}$	1.49(15) 1.45	1.63(14) 1.62	1.65(28) 1.75	1.76(18) 1.86		17.0 29.3		1.58(11) 1.44	

Table 2: (continued)

nucleus	$\frac{4_1 \rightarrow 2_1}{2_1 \rightarrow 0_1}$	$\frac{6_1 \rightarrow 4_1}{2_1 \rightarrow 0_1}$	$\frac{8_1 \rightarrow 6_1}{2_1 \rightarrow 0_1}$	$\frac{10_1 \rightarrow 8_1}{2_1 \rightarrow 0_1}$	$\frac{2_\beta \rightarrow 0_1}{2_1 \rightarrow 0_1}$ x $10^3$	$\frac{2_\beta \rightarrow 2_1}{2_1 \rightarrow 0_1}$ x $10^3$	$\frac{2_\beta \rightarrow 4_1}{2_1 \rightarrow 0_1}$ x $10^3$	$\frac{2_\gamma \rightarrow 2_1}{2_\gamma \rightarrow 0_1}$	$\frac{2_\gamma \rightarrow 4_1}{2_\gamma \rightarrow 0_1}$
$^{174}\text{Hf}$					14(4)		9(3)	1.54(76)	
	1.48	1.74	1.96	2.20	24.8	52.5	185	1.49	0.0801
$^{176}\text{Hf}$					5.4(11)		31(6)		
	1.47	1.71	1.91	2.11	23.5	47.4	157	1.48	0.0791
$^{178}\text{Hf}$		1.38(9)	1.49(6)	1.62(7)	0.4(2)		2.4(9)	1.13(17)	0.066(10)
	1.47	1.70	1.90	2.10	23.3	46.7	153	1.47	0.078
$^{180}\text{Hf}$	1.48(20)	1.41(15)	1.61(26)	1.55(10)				1.34(28)	
	1.48	1.73	1.95	2.17	24.5	51.1	177	1.48	0.0795
$^{182}\text{W}$	1.43(8)	1.46(16)	1.53(14)	1.48(14)	6.6(6)	4.6(6)	13(1)	1.98(7)	0.010(1)
	1.48	1.72	1.93	2.15	24.1	49.6	169	1.48	0.0787
$^{184}\text{W}$	1.35(12)	1.54(9)	2.00(18)	2.45(51)	1.8(3)		24(3)	1.91(13)	0.109(9)
	1.50	1.79	2.07	2.37	26.5	61.4	240	1.50	0.0814
$^{186}\text{W}$	1.30(9)	1.69(12)	1.60(12)	1.36(36)				2.18(15)	
	1.52	1.85	2.18	2.53	27.3	69.0	294	1.51	0.0829
$^{186}\text{Os}$	1.45(7)	1.99(7)	1.89(11)	2.06(44)				2.33(12)	0.12(4)
	1.52	1.86	2.19	2.55	27.3	70.0	301	1.51	0.0830
$^{188}\text{Os}$	1.68(11)	1.75(11)	2.04(15)	2.38(32)				3.20(6)	6.8(13)
	1.53	1.86	2.20	2.56	27.4	70.7	307	1.50	0.0810
$^{230}\text{Th}$	1.36(8)				5.7(26)		20(11)	1.8(8)	0.12(8)
	1.48	1.72	1.94	2.16	24.3	50.2	172	1.48	0.0797
$^{232}\text{Th}$	1.44(15)	1.65(14)	1.73(12)	1.82(15)	14(6)	2.6(13)	17(8)	2.48(42)	0.045(20)
	1.46	1.68	1.85	2.03	21.9	42.0	130	1.46	0.0770
$^{234}\text{U}$								1.69(40)	0.097(24)
	1.45	1.64	1.78	1.91	19.0	34.0	95	1.45	0.0751
$^{236}\text{U}$	1.42(11)	1.55(11)	1.59(17)	1.46(17)					
	1.45	1.63	1.76	1.88	17.8	31.3	85	1.45	0.0743
$^{238}\text{U}$			1.45(23)	1.71(22)	1.4(6)	3.6(14)	12(5)	1.74(17)	0.108(12)
	1.45	1.63	1.75	1.87	17.3	30.1	95 80	1.45	0.0743
$^{238}\text{Pu}$					14(4)		11(4)		
	1.45	1.63	1.75	1.86	17.2	29.8	79	1.45	0.0741
$^{250}\text{Cf}$								1.61(27)	0.092(16)
	1.44	1.61	1.72	1.81	14.8	24.7	61	1.44	0.0730

Table 3: Values of  $\beta_0$  (determined through minimization of  $\sigma_{\beta,\gamma}$  [Eq. (15)] and  $C$  [determined through Eq. (14)] corresponding to minimum rms deviation  $\sigma_{\beta,\gamma}$  [Eq. (15)] between the  $\beta_1$  and  $\gamma_1$  bands of the ES-D solution for fixed value of  $R_{0/2}$ , when the even levels of both bands up to  $L_{max}$  are taken into account. See subsection 3.7 for further discussion.

$R_{0/2}$	$L_{max}$	$\beta_0$	$C$	$\sigma_{\beta,\gamma}$
5.	10	0.00	1.0	5.026
10.	10	0.00	7.3	3.072
15.	10	1.94	12.9	1.141
20.	10	2.64	16.1	0.993
25.	10	3.12	19.4	0.907
30.	10	3.53	22.2	0.855
5.	20	0.00	1.0	4.890
10.	20	0.00	7.3	4.528
15.	20	1.73	14.7	2.611
20.	20	2.57	17.7	2.531
25.	20	3.09	20.6	2.371
30.	20	3.50	23.9	2.197

Table 4: Theoretical predictions of the ES-D solution for  $\beta_0 = 1.95$  and  $C = 12.9$  compared to experimental data for  $^{232}\text{Th}$  [45]. See subsection 3.7 for further discussion.

$L$	gsb exp	gsb th	$\beta_1$ exp	$\beta_1$ th	$L$	$\gamma_1$ exp	$\gamma_1$ th
0	0.000	0.000	14.794	15.021	2	15.907	17.210
2	1.000	1.000	15.680	16.021	3	16.804	17.978
4	3.284	3.268	17.683	18.288	4	18.030	18.989
6	6.749	6.665	20.724	21.686	5	19.454	20.234
8	11.280	11.021	24.754	26.042	6	21.266	21.701
10	16.751	16.161	29.762	31.182	7	23.213	23.379
12	23.033	21.931	35.549	36.952	8	25.496	25.254
14	30.035	28.200	42.138	43.221	9	27.750	27.313
16			49.438	49.887	10	30.624	29.542
18			57.356	56.868	11	33.219	31.929
20			65.811	64.102	12	36.484	34.461